Electronic Supplementary Material (ESI) for ChemComm.

Supporting Information

1. Experimental

A) General Methods and Instrumentation

All manipulations were carried out under argon atmosphere using standard Schlenk or glovebox techniques and glassware was flame-dried before use. Unless otherwise stated, all chemicals were purchased from Sigma-Aldrich or ABCR and used as received. All solvents were refluxed over sodium/benzophenone, distilled, and deoxygenated before use.

Deuterated benzene (C_6D_6), deuterated chloroform ($CDCl_3$) and deuterated THF (THF-d_8) were obtained from Sigma-Aldrich and were dried over 3 Å molecular sieves. All NMR samples were prepared under argon in J. Young PTFE tubes. Nitrogen monoxide (5.0) was purchased from Westfalen AG and used as received. 1,3-bis(2,6-diisopropyl phenyl)-2-methylene-2,3-dihydro-1H-imidazole (^{Dipp}NHO), $KSi(TMS)_3$, $KSi(TMS)_2Si(iPr)_3$ and Cl-Si(tolyl)$_3$ were synthesized according to literature procedures.[1,2]

NMR spectra were recorded on Bruker AV-500C and AV-400 spectrometers at ambient temperature (300 K). ^{1}H, ^{13}C, HMBC, and ^{29}Si NMR spectroscopic chemical shifts δ are reported in ppm relative to tetramethylsilane. δ(^{1}H) and δ(^{13}C) were referenced internally to the relevant residual solvent resonances. δ(^{29}Si) was referenced to the signal of tetramethylsilane (TMS) (δ = 0 ppm) as an external standard.

Liquid Injection Field Desorption Ionization Mass Spectroscopy (LIFDI-MS) was measured directly from an inert atmosphere glovebox with a Thermo Fisher Scientific Exactive Plus Orbitrap equipped with an ion source from Linden CMS.[3] Melting points (m.p.) were measured in sealed glass capillaries under argon atmosphere using a Büchi B-540 melting point apparatus.

Infrared (IR) spectra were recorded on a Perkin Elmer FT-IR spectrometer (diamond ATR, Spectrum Two) in the range of 400–4000 cm^{-1} at room temperature under an argon atmosphere. IR intensity bands are abbreviated as s = strong, m = medium, and w = weak.

UV-Vis spectra were recorded on Agilent Cary 60 UV-Vis spectromether in hexane or thf solution.

B) Experimental procedures

Modified literature synthesis of diazoolefin A-1

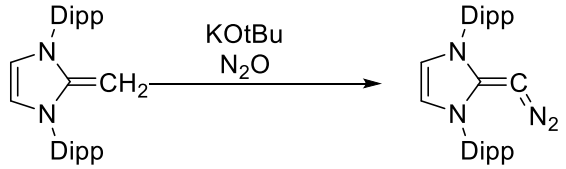

A-1

A-1 was synthesized by a modified route of *Severin et al.* 2.00 g N-heterocyclic olefin ^{Dipp}NHO (4.97 mmol, 1.00 eq.) and 0.57g KO^{t}Bu (4.97 mmol, 1.00 eq.) were dissolved in 50mL DMF in a flame dried pressure Schlenk flask. The reaction mixture was degassed by two freeze-pump-thaw cycles and pressurized with N_2O (1 atm). The solution was heated to 50°C and stirred for three hours, whereas a color change from orange to dark red could be observed. The reaction mixture was allowed to cool to 40°C, and DMF was evaporated under reduced pressure at this temperature. The crude product mixture was washed with Et_2O (10 mL) and pentane (80 mL) and afterwards extracted with THF (80 mL). THF was evaporated under reduced pressure and after additional washing with pentane (20 mL) the product ^{Dipp}NHO-N_2 (**A-1**) was obtained as a yellow to red powder (1.72 g, 3.98 mmol, 80%). Analytical data matched with literature-known data.[4] For completeness, a reference ^{1}H-NMR spectrum in THF was attached.

^{1}H NMR (400 MHz, THF-d_8, 300 K): δ[ppm]= 7.40 (t, 2H, $^{3}J_{H,H}$ = 7.8 Hz, Ar-*H*), 7.25 (d, 4H, $^{3}J_{H,H}$ = 7.8 Hz, Ar-*H*), 6.88 (s, 2H, NC*H*), 2.93 (hept, 4H, $^{3}J_{H,H}$ = 6.9 Hz, C*H*$(CH_3)_2$), 1.32 (d, 12H, $^{3}J_{H,H}$ = 6.9 Hz, CH(C*H*$_3)_2$), 1.24 (d, 12H, $^{3}J_{H,H}$ = 6.9 Hz, CH(C*H*$_3)_2$).

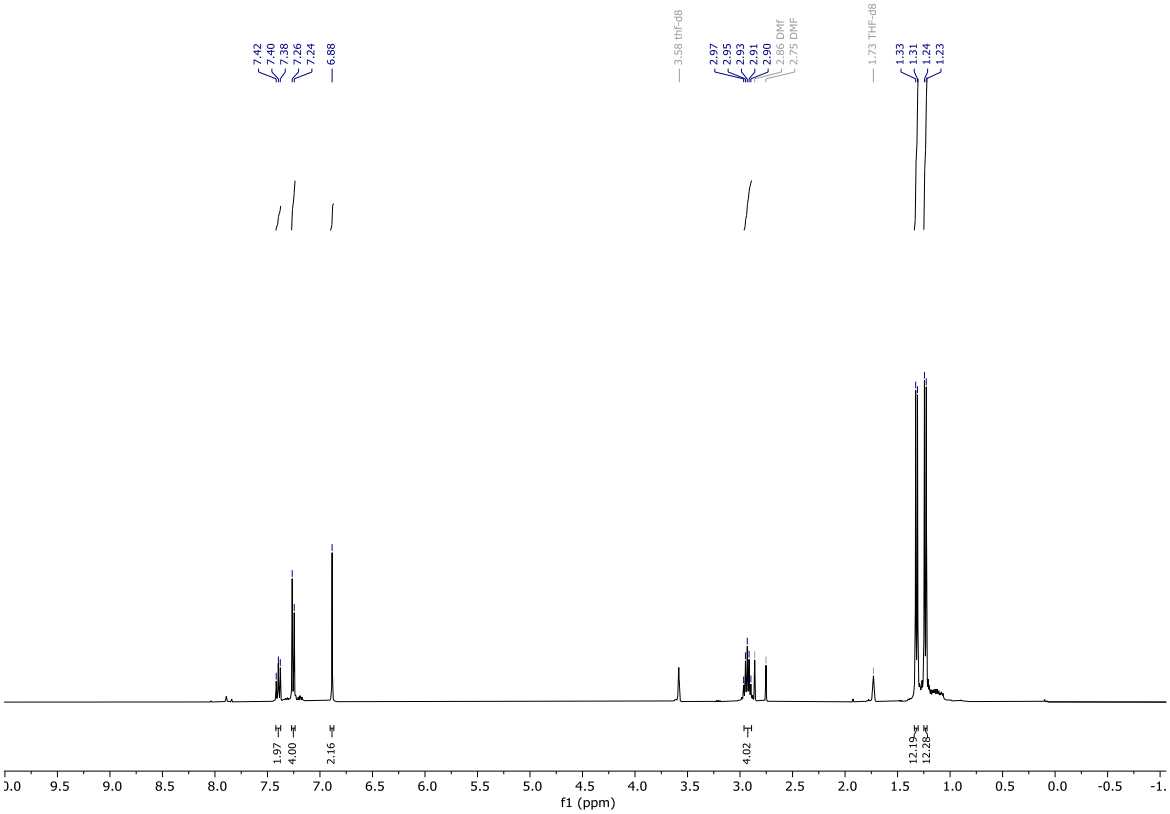

Figure S1: ^{1}H-NMR spectrum of diazoolefin **A-1** in THF-d_8.

Synthesis of germanium complex ^{Dipp}NHO-N_2-$GeCl_2$ (1):

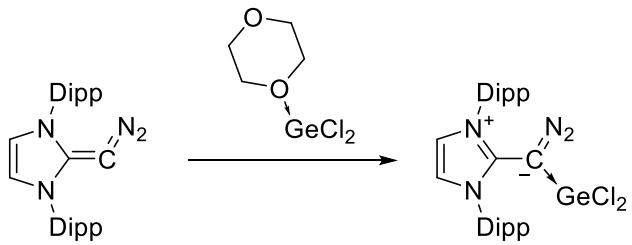

A-1 **1**

At room temperature, 5.00 mL diethylether were added to 108.10 mg GeCl2 dioxane (0.47 mmol, 1.00 eq.) and 200 mg DippNHO-N2 (0.47 mmol). The suspension was stirred for 3 hours, whereas the reaction mixture turned from brown-red to beige. The solution was filtered, and the filtrate was washed twice with 3.00 mL of diethyl ether. After drying the solid in a vacuum, the product ^{Dipp}NHO-N_2-$GeCl_2$ was obtained as a beige solid in 79% yield (150 mg, 0.37 mmol). In most cases, approx 6 mol% of a non-fully characterized side product can be observed. Crystals suitable for SC-XRD measurement were grown from a concentrated THF solution of the product at -35°C.

^{1}H NMR (400 MHz, THF-d_8, 300 K): δ[ppm]= 7.57 (t, 2H, $^{3}J_{H-H}$ = 7.9 Hz, Ar-*H*), 7.46 (s, 2H, NC*H*), 7.39 (d, 4H, $^{3}J_{H-H}$ = 7.9 Hz, Ar-*H*), 2.75 (hept, 4H, $^{3}J_{H-H}$ = 6.9 Hz, C*H*(CH_3)$_2$), 1.34 (d, 12H, $^{3}J_{H-H}$ = 6.9 Hz, CH(C*H*$_3$)$_2$), 1.24 (d, 12H,$^{3}J_{H-H}$ = 6.9 Hz, CH(C*H*$_3$)$_2$).

^{13}C-NMR (100 MHz, THF-d_8, 300 K): δ[ppm]= 149.8 (*C*-imidazole), 147.9 (Ar-*C*), 133.0 (Ar-*C*), 132.3 (Ar-*C*), 125.9 (C-Ar), 122.9 (N*C*H), 50.7 (*C*-N_2), 30.2 (C*H*(CH_3)$_2$), 24.9 (CH(C*H*$_3$)$_2$), 23.6 (CH(C*H*$_3$)$_2$).

^{1}H NMR (400 MHz, $CDCl_3$, 300 K): δ[ppm]= 7.56 (t, 2H, $^{3}J_{H-H}$ = 7.9 Hz Ar-*H*), 7.33 (d, 4H, $^{3}J_{H-H}$ = 7.9 Hz Ar-*H*), 6.96 (s, 2H, NC*H*), 2.67 (hept, 4H, $^{3}J_{H-H}$ = 6.9 Hz, C*H*$(CH_3)_2$), 1.34 (d, 12H, $^{3}J_{H-H}$ = 6.9 Hz, CH(C*H*$_3)_2$), 1.23 (d, 12H, $^{3}J_{H-H}$ = 6.9 Hz, CH(C*H*$_3)_2$).

^{13}C-NMR (100 MHz, $CDCl_3$, 300 K): δ[ppm]= 149.2 (*C*-imidazole), 146.9 (Ar-*C*), 132.5 (Ar-*C*), 130.6 (Ar-*C*), 125.3 (C-Ar), 120.7 (N*C*H), 50.5 (*C*-N_2), 29.3 (C*H*$(CH_3)_2$), 24.8 (CH(C*H*$_3)_2$), 23.2 (CH(C*H*$_3)_2$).

IR (solid): $\tilde{\nu}$ [cm^{-1}] = 2964 (m), 2039 (s) ($\tilde{\nu}$-N_2), 1503 (s), 1468 (m), 805(m)

UV-Vis: λmax = 320 nm (ε = 1110 L mol^{-1} cm^{-1})

m.p.: 190-192 °C (decomposition)

LIFDI-MS: Compound 1 could not be observed in MS spectra.

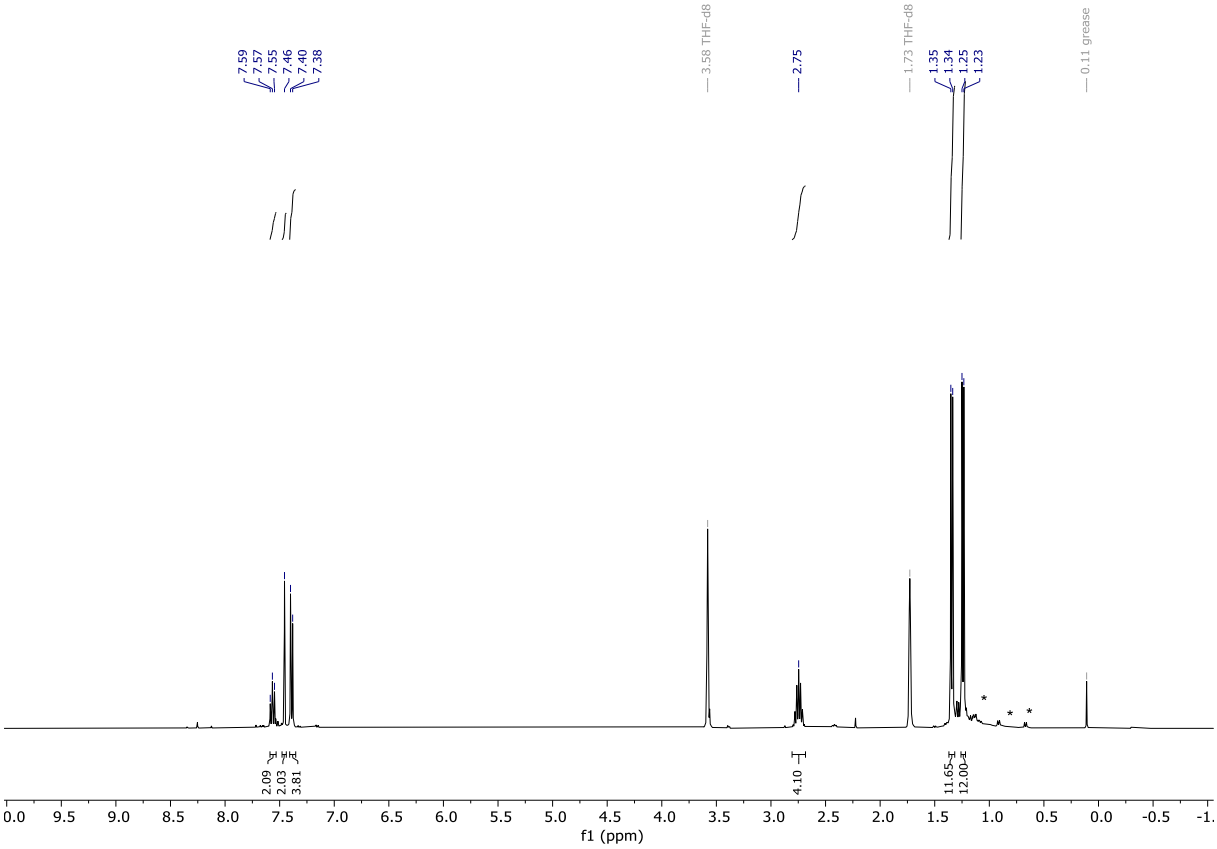

Figure S2: ^{1}H-NMR of germanium complex **1** in THF-d_8. Signals of impurity **1'** marked with *.

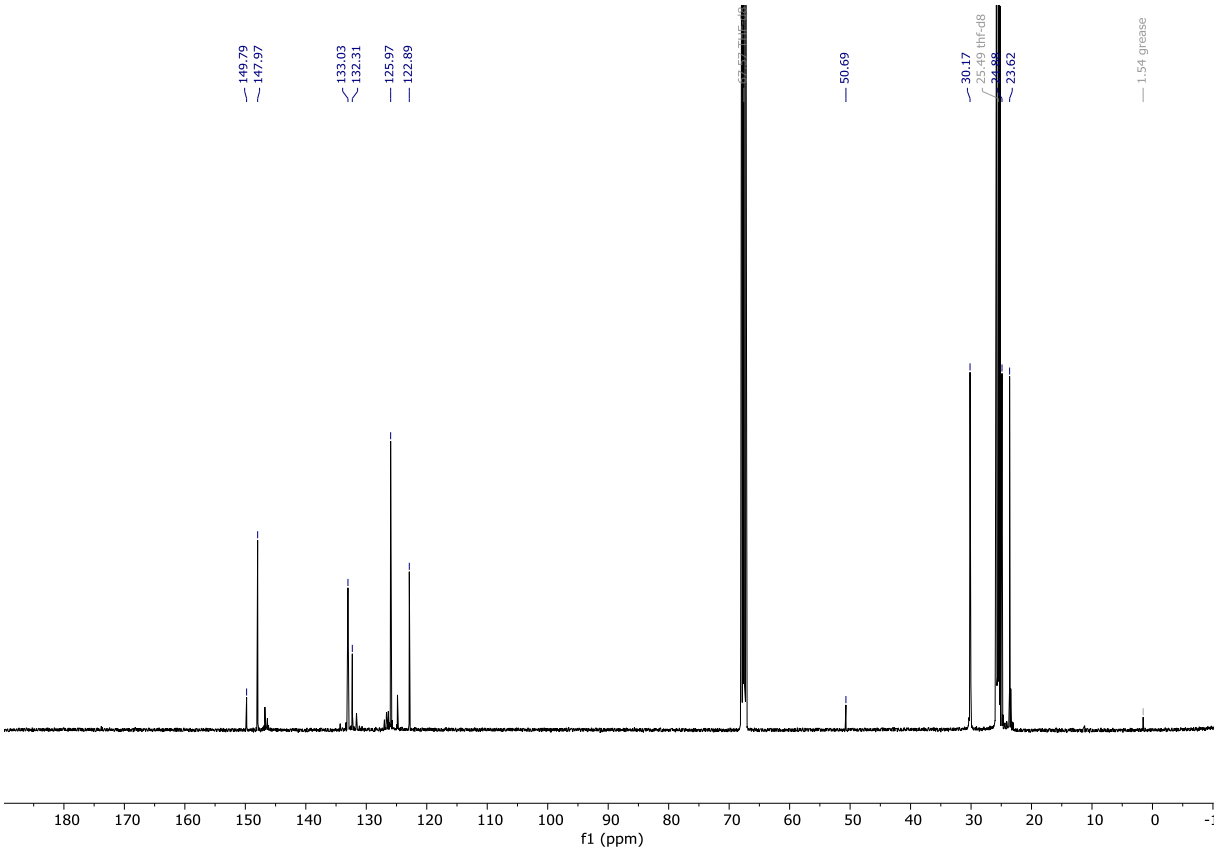

Figure S3: ^{13}C-NMR spectrum of germanium complex **1** in THF-d_8.

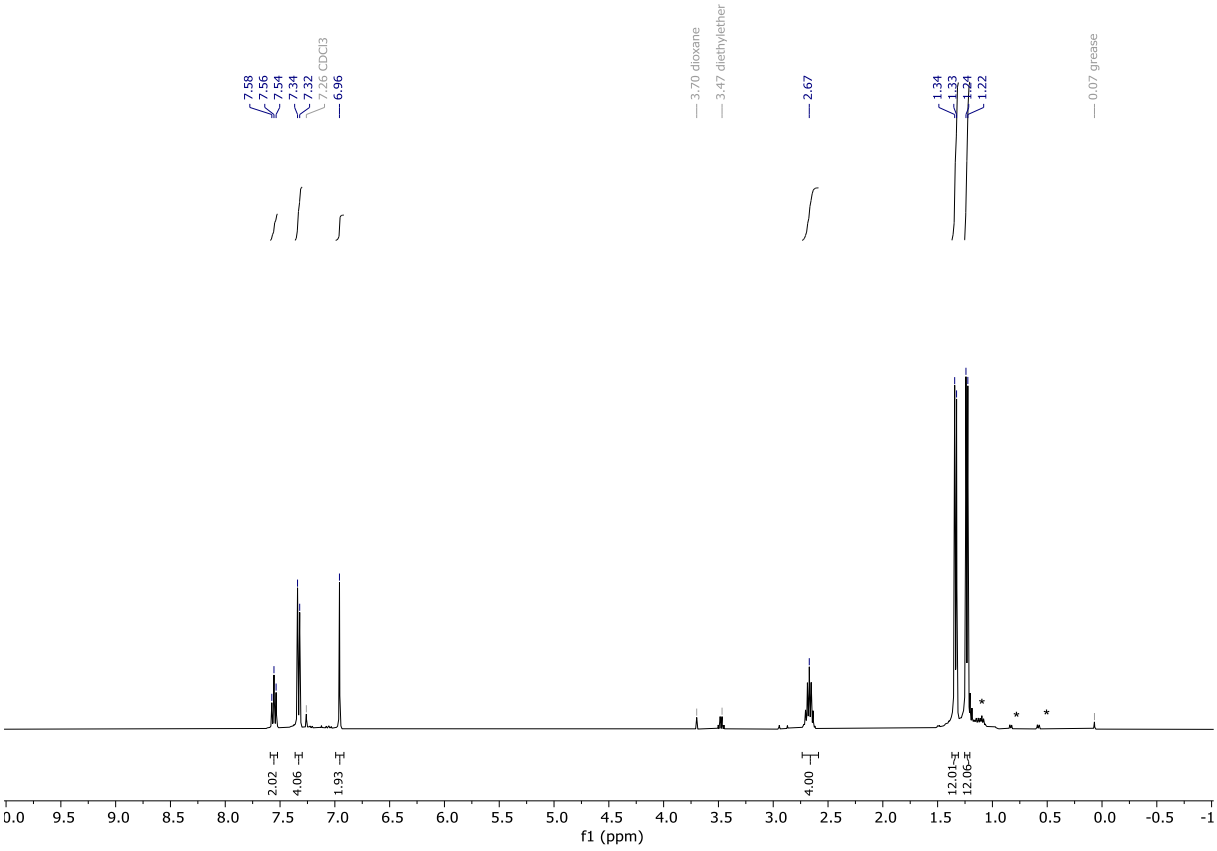

Figure S4: ^{1}H-NMR spectrum of germanium complex **1** in $CDCl_3$. Signals of impurity **1'** marked with *.

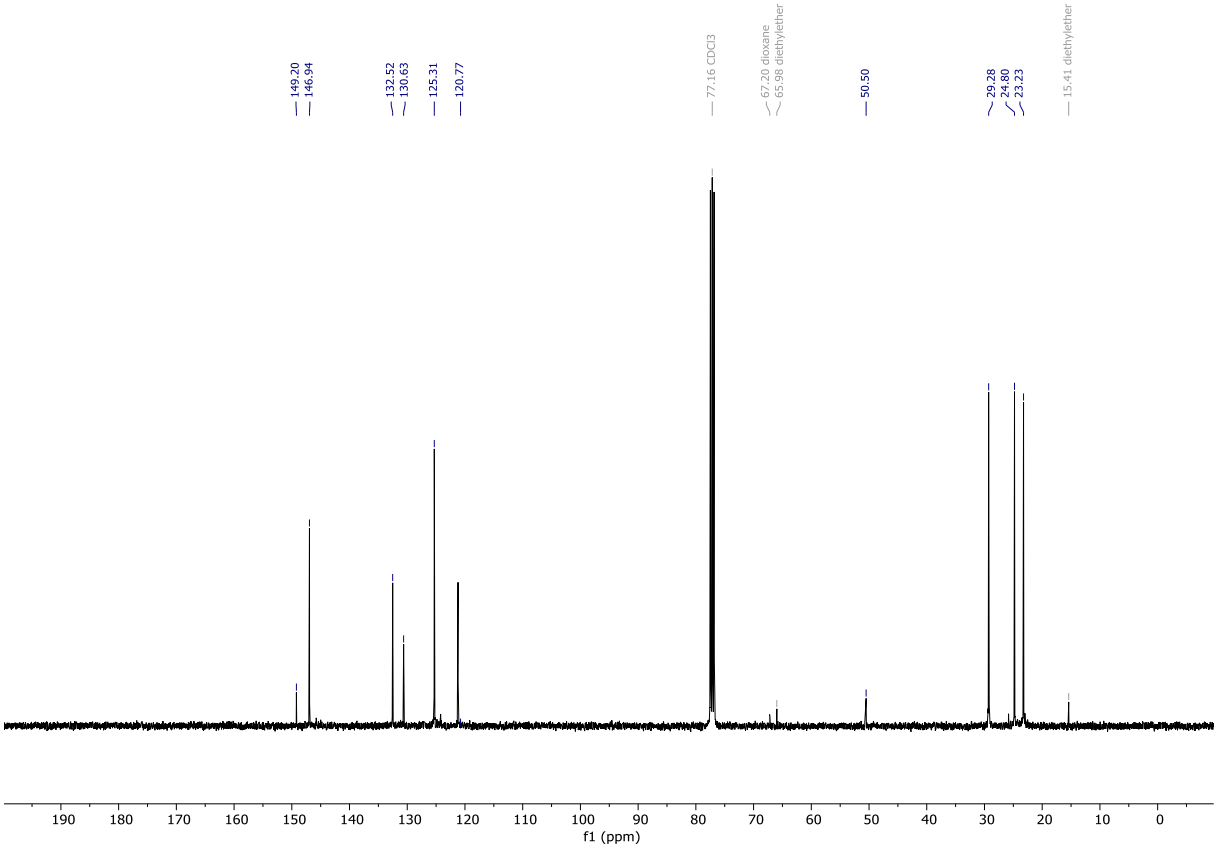

Figure S5: ^{13}C-NMR spectrum of germanium complex **1** in $CDCl_3$.

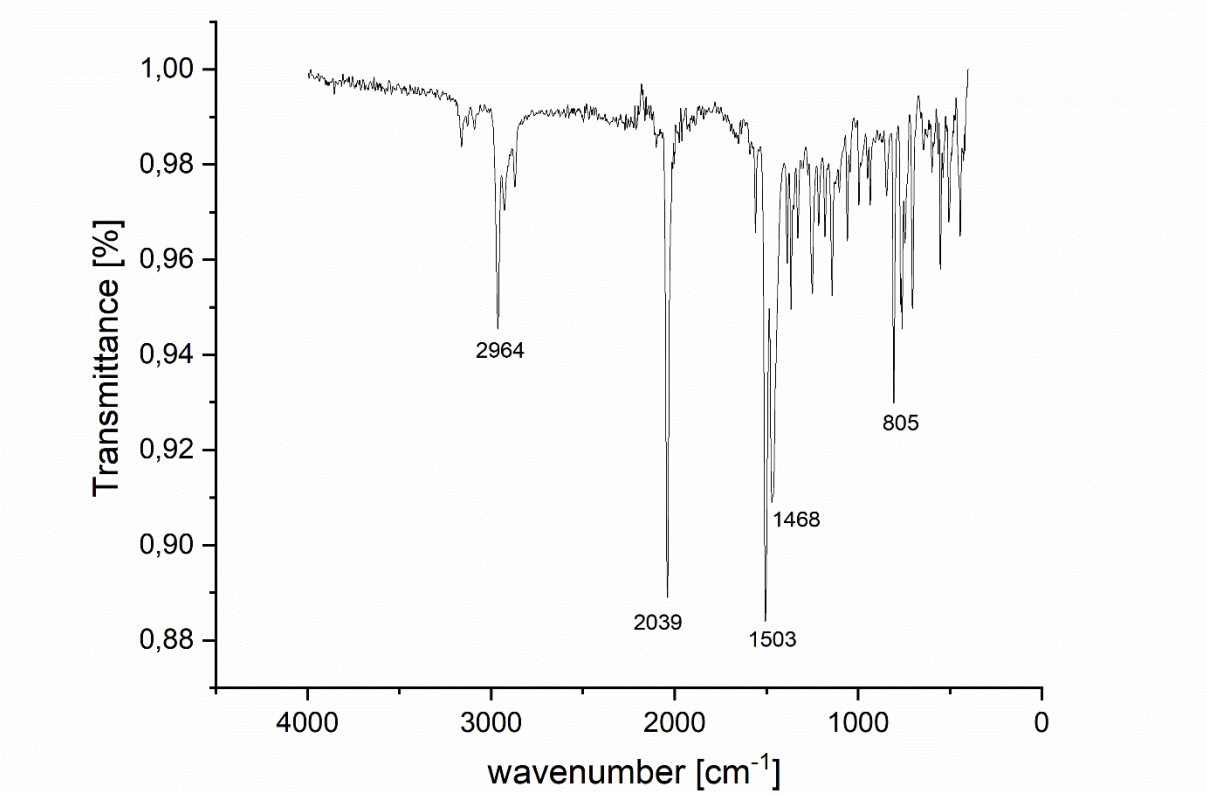

Figure S6: IR spectrum (solid) of germanium complex **1**.

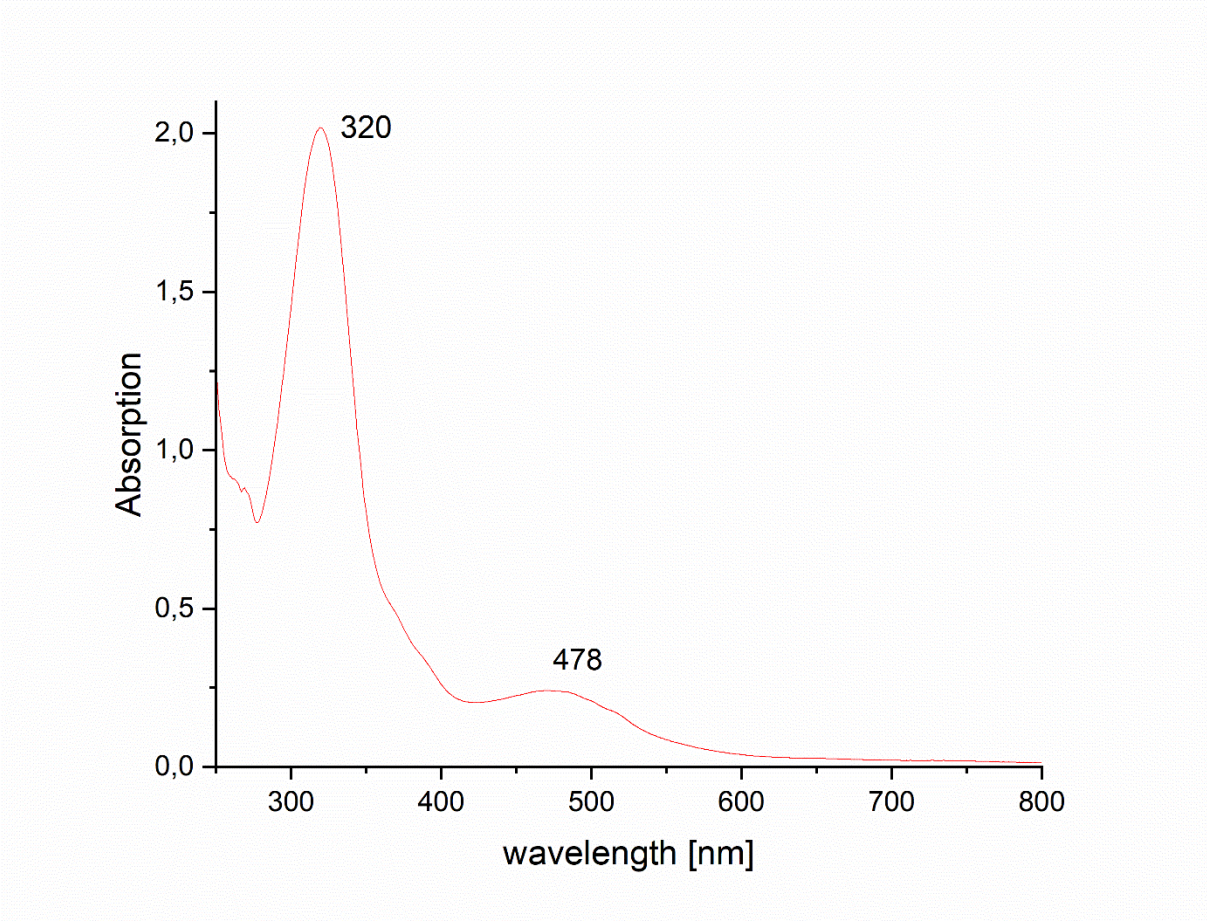

Figure S7: UV-Vis spectrum of compound **1** in THF; c = 1.9 mM.

Synthesis of tin complex ^{Dipp}NHO-N_2-$SnCl_2$ (2):

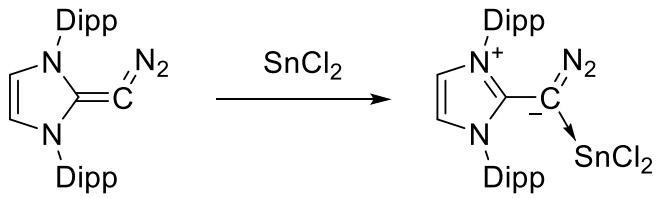

A-1 **2**

At room temperature, 5.00 mL diethylether were added to 88.47 mg SnCl2 (0.47 mmol, 1.00 eq.) and 200 mg DippNHO-N2 (0.47 mmol). The suspension was stirred for 4 hours, whereas the reaction mixture turned from brown-red to beige. The solution was filtered, and the filtrate was washed twice with 3.00 mL of diethyl ether. After drying the solid in a vacuum, the product ^{Dipp}NHO-N_2-$SnCl_2$ was obtained as a beige solid in 68% yield (194 mg, 0.32 mmol). In most cases, approx. 5 mol% of a non-fully characterized side product can be observed. Crystals suitable for SC-XRD measurement were grown from a concentrated THF solution of the product at -35°C.

^{1}H NMR (400 MHz, THF-d_8, 300 K): δ[ppm]= 7.57 (t, 2H, $^3J_{H-H}$ = 7.9 Hz, Ar-*H*), 7.45 (s, 2H, NC*H*), 7.41 (d, 4H, $^3J_{H-H}$ = 7.9 Hz, Ar-*H*), 2.75 (hept, 4H, $^3J_{H-H}$ = 6.9 Hz, C*H*(CH_3)$_2$), 1.35 (d, 12H, $^3J_{H-H}$ = 6.9 Hz, CH(C*H*$_3$)$_2$), 1.25 (d, 12H, $^3J_{H-H}$ = 6.9 Hz, CH(C*H*$_3$)$_2$).

^{13}C-NMR (100 MHz, THF-d_8, 300 K): δ[ppm]= 151.3 (*C*-imidazole), 148.2 (Ar-*C*), 133.1 (Ar-*C*), 132.3 (Ar-*C*), 126.2 (C-Ar), 122.5 (N*C*H), 53.8 (*C*-N_2), 30.2 (C*H*(CH_3)$_2$), 24.8 (CH(C*H*$_3$)$_2$), 23.8 (CH(C*H*$_3$)$_2$).

^{1}H NMR (400 MHz, $CDCl_3$, 300 K): δ[ppm]= 7.55 (t, 2H, $^3J_{H-H}$ = 7.9 Hz, Ar-*H*), 7.35 (d, 4H, $^3J_{H-H}$ = 7.9 Hz, Ar-*H*), 6.95 (s, 2H, NC*H*), 2.68 (hept, 4H, $^3J_{H-H}$ = 6.9 Hz, C*H*(CH_3)$_2$), 1.35 (d, 12H, $^3J_{H-H}$ = 6.9 Hz, CH(C*H*$_3$)$_2$), 1.24 (d, 12H, $^3J_{H-H}$ = 6.9 Hz, CH(C*H*$_3$)$_2$).

^{13}C-NMR (400 MHz, $CDCl_3$, 300 K): δ[ppm]= 150.9 (*C*-imidazole), 147.5 (Ar-*C*), 132.9 (Ar-*C*), 131.0 (Ar-*C*), 125.9 (C-Ar), 121.1 (N*C*H), 54.6 (*C*-N_2), 29.6.2 (C*H*(CH_3)$_2$), 25.1 (CH(C*H*$_3$)$_2$), 23.8 (CH(C*H*$_3$)$_2$).

^{119}Sn-NMR (150 MHz, $CDCl_3$, 300 K): δ[ppm]= -36.6.

IR (solid): $\tilde{\nu}$ [cm^{-1}] = 2964 (m), 2039 (s) ($\tilde{\nu}$-N_2), 1506 (s), 1464 (m), 803(m).

UV-Vis: λmax = 320 nm (ε = 844 L mol^{-1} cm^{-1})

m.p.: 193-197 °C (decomposition).
LIFDI-MS: Compound **2** could not be observed in MS spectra.

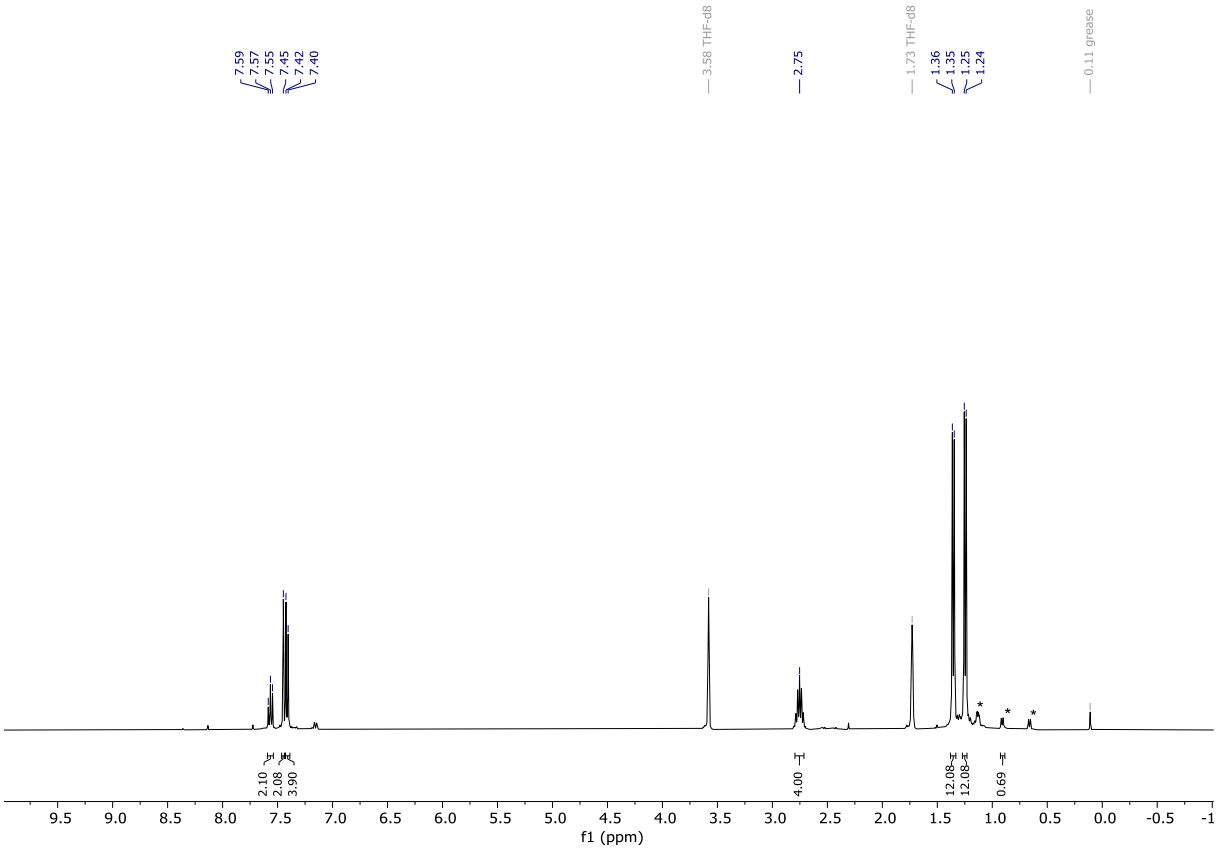

Figure S8: ^{1}H-NMR spectrum of tin complex **2** in THF-d_8. Signals of impurity **2'** marked with *.

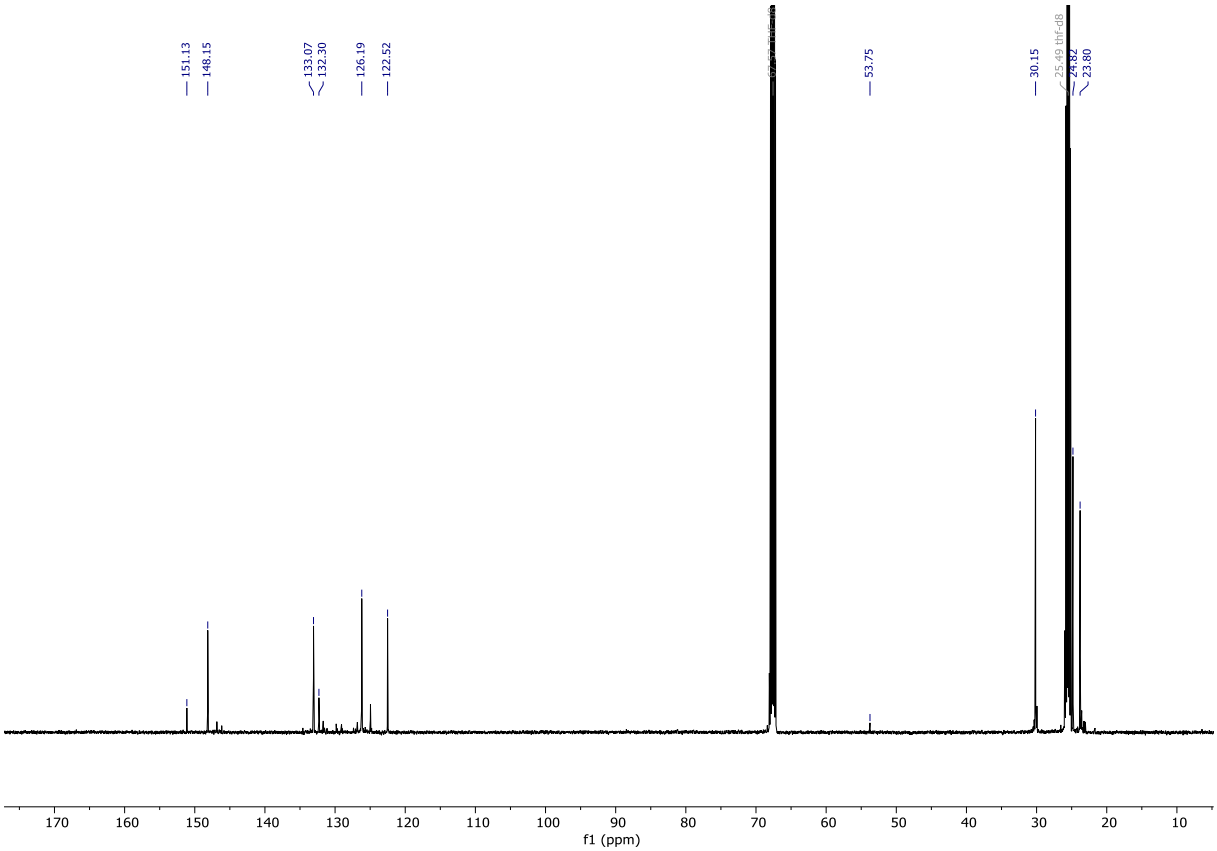

Figure S9: ^{13}C-NMR spectrum of tin complex **2** in THF-d_8.

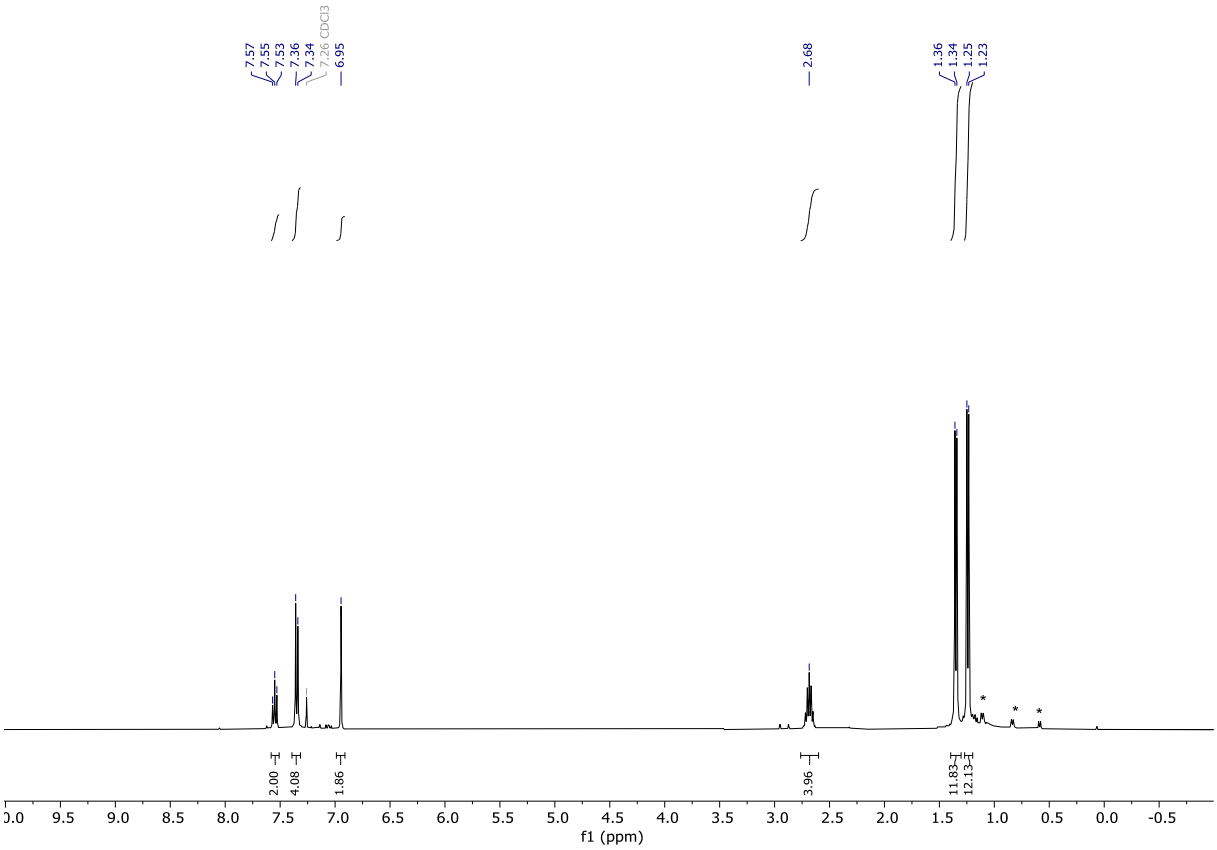

Figure S10: ^{1}H-NMR spectrum of tin complex **2** in $CDCl_3$.

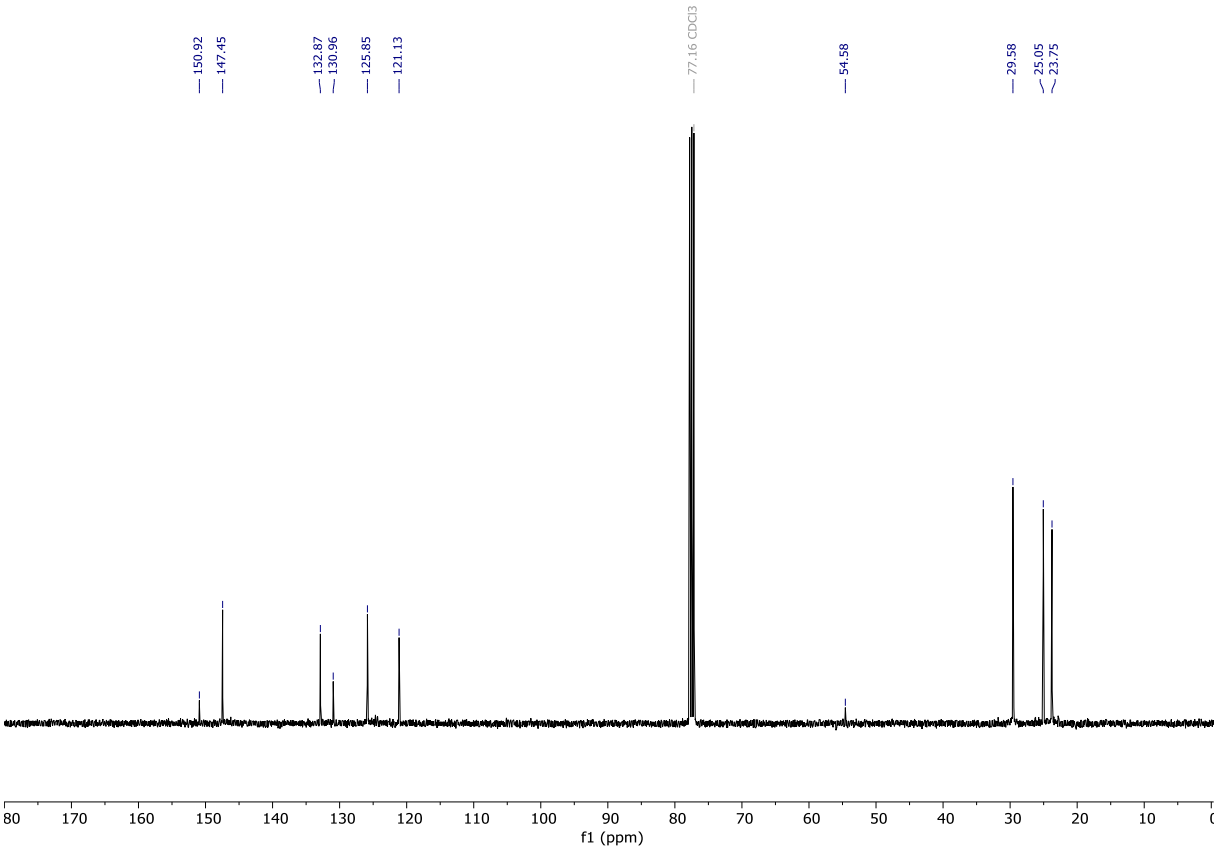

Figure S11: ^{13}C-NMR spectrum of tin complex **2** in $CDCl_3$.

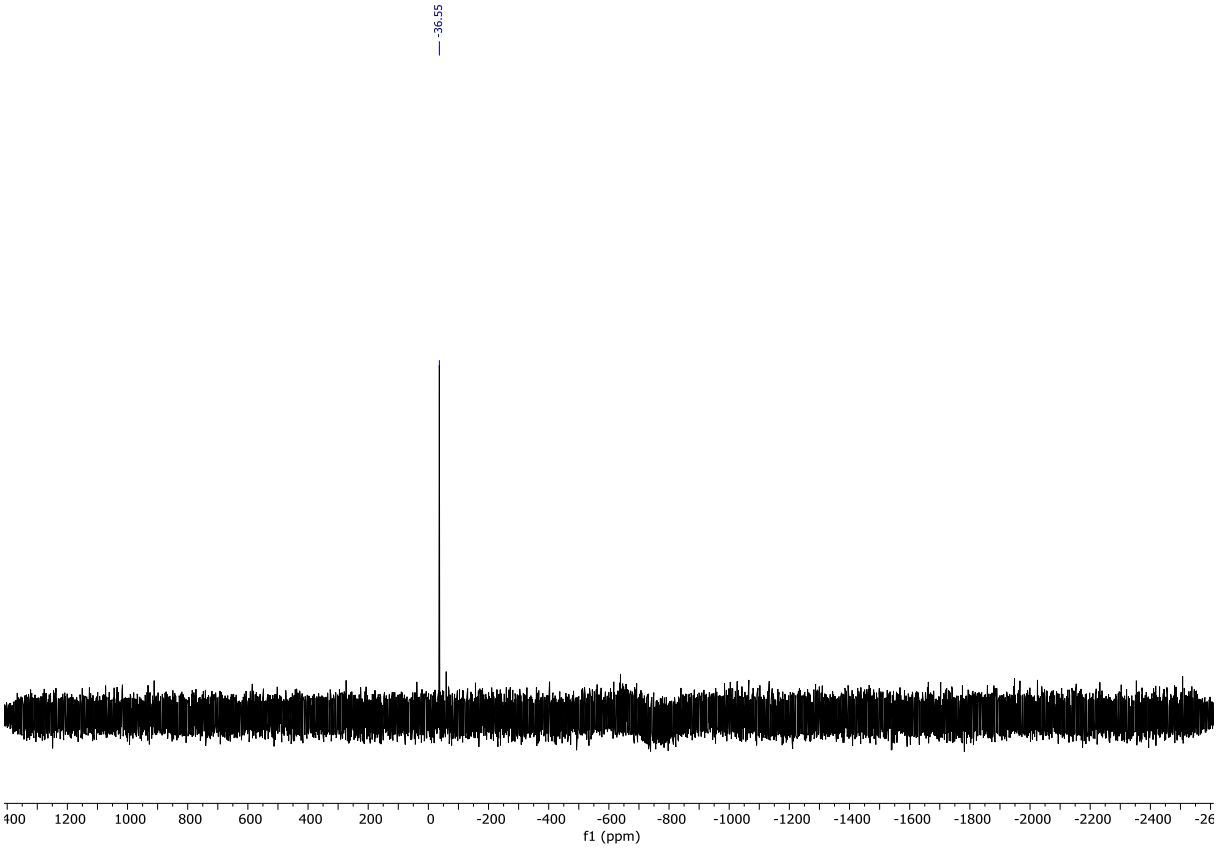

Figure S12: ^{119}Sn-NMR spectrum of tin complex **2** in THF-d_8

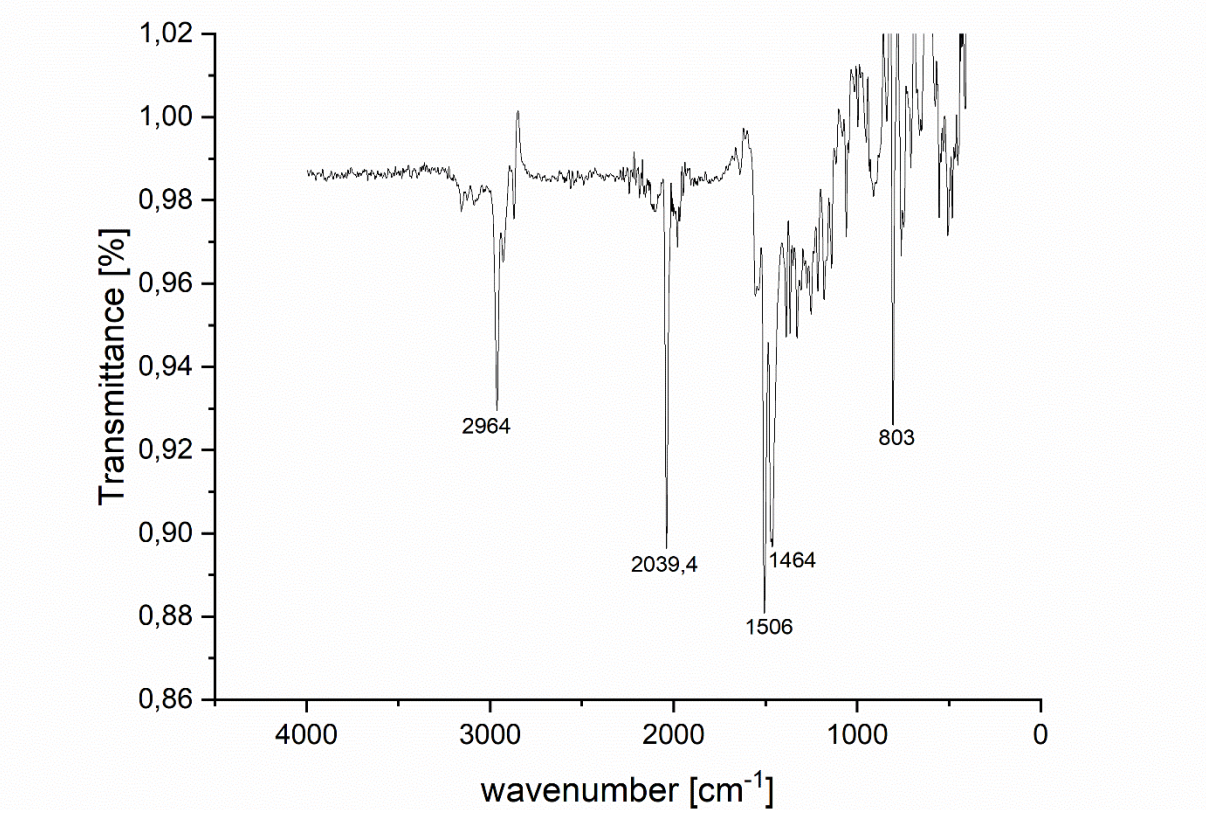

Figure S13: IR spectrum (solid) of tin complex 2.

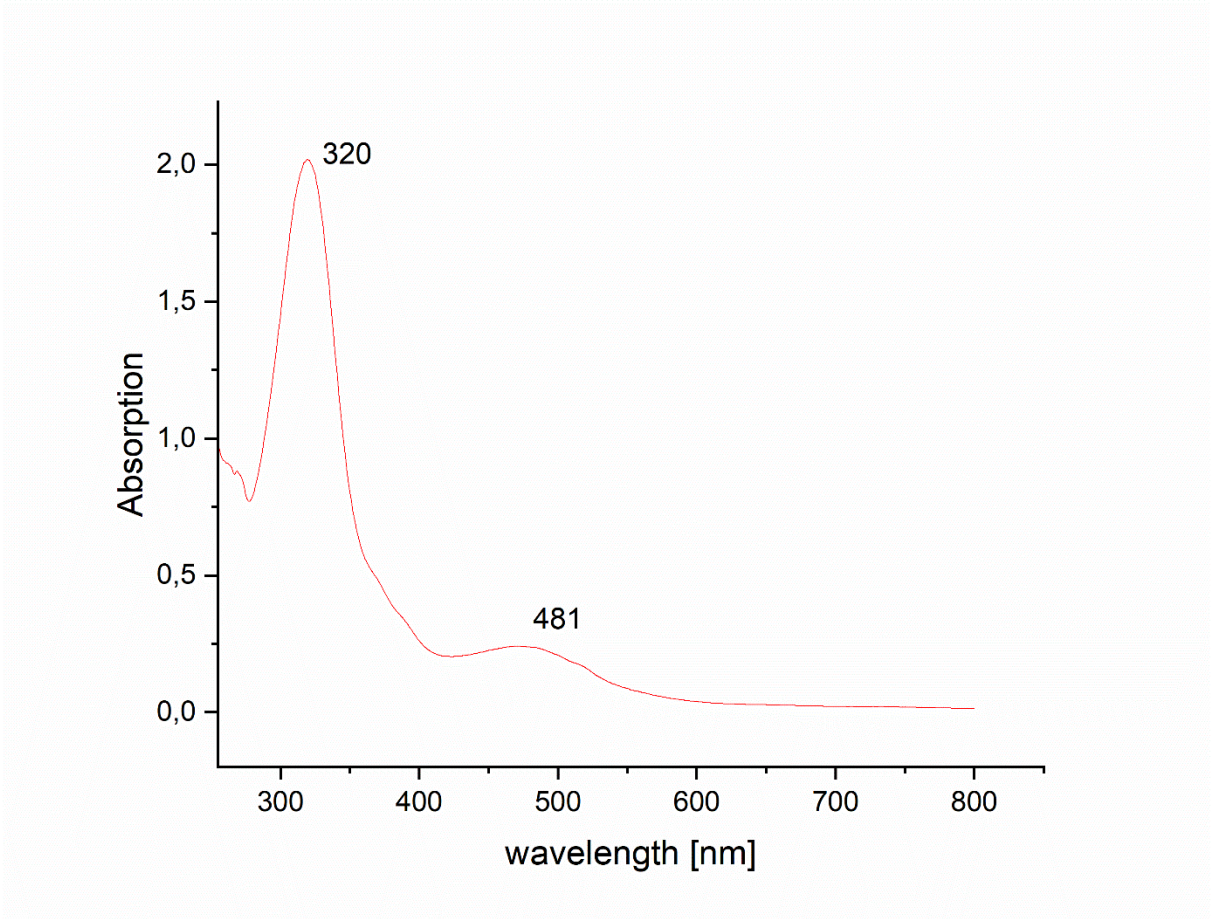

Figure S14: UV-Vis spectrum of compound **2** in THF; c = 2.5 mM.

Fomation of non-fully charactized side products in the synthesis of 1 and 2

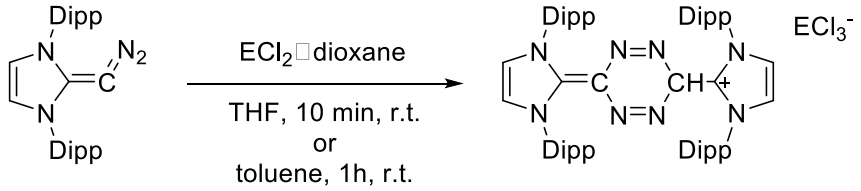

A-1

1': E = Ge
2': E = Sn

Stirring of a solution of Diazoolefin **A-1** and ECl_2 dioxane in THF for 10 min leads to the predominant formation of a non-fully characterized compound **1'** or **2'** as the main product (approx. 60 – 70% according to NMR) instead of the formation of **1** or **2**. Alternatively, a solution of diazoolefin **A-1** in toluene can be added to a suspension of $GeCl_2$ dioxane in toluene/benzene and stirred for 1h. After removal of the solvents NMR analysis in $CDCl_3$ shows the formation of **1'** and **2'**in both cases. Due to the instable nature of this compound, a proper isolation was not achieved so far. Different purification methods failed as the compound decomposes unselectively in various solvents and as solid at room temperature within 1 day. Crystallization of a small fraction (about 3% total yield) of **1'** in a concentrated thf solution at -35°C in poor quality could be achieved. Crystallization of **2'** was not successful.

NMR data of 1':

^{1}H NMR (400 MHz, THF-d_8, 300 K): δ[ppm]= 8.15 (s, 2H, NCH), 7.73 (s, 2H, imidazole-NC*H*), 7.40 (m, 4H, Ar-*H*), 7.16 (d, 8H, $^3J_{H-H}$ = 7.8 Hz, Ar-*H*), 2.54 (m, 4H, C*H*$(CH_3)_2$), 2.44 (m, 4H, C*H*$(CH_3)_2$), 1.51 (s, 1H, N_2-CH 1.14 (dd, 24 H, $^3J_{H-H}$ = 6.9 Hz, Imidazol-CH(C*H*$_3)_2$), 0.92 (d, 12H, $^3J_{H-H}$ = 6.7 Hz, CH(C*H*$_3)_2$), 0.67(d, 12H, $^3J_{H-H}$ = 6.8 Hz, CH(C*H*$_3)_2$).

^{13}C-NMR (100 MHz, THF-d_8, 300 K): δ[ppm]= 148.4 (*C*-imidazole), 147.1 (NCH) 146.4 (NCH), 138.8 (C-imidazole),133.3 (Ar-C), 130.0 (Ar-*C*), 129.3 (Ar-*C*), 126.4 (C-Ar), 126.4 (Ar-C), 125.2 (Ar-C), 125.1 (Ar-C), 122.9 (Ar-C), 30.5 (*C*-N_2), 30.3 (C*H*$(CH_3)_2$), 30.2 (*C*H-N_2), 25.1 (*C*H$(CH_3)_2$), 24.0 (CH(C*H*$_3)_2$), 23.5 (CH(C*H*$_3)_2$), 23.3 (CH(C*H*$_3)_2$), 21.9 (CH(C*H*$_3)_2$).

NMR data of 2':

^{1}H NMR (400 MHz, THF-d_8, 300 K): δ[ppm]= 8.16 (s, 2H, NCH), 7.73 (s, 2H, imidazole-NC*H*), 7.39 (m, 4H, Ar-*H*), 7.15 (d, 8H, $^3J_{H-H}$ = 7.8 Hz, Ar-*H*), 2.54 (m, 4H, C*H*$(CH_3)_2$), 2.44 (m, 4H, C*H*$(CH_3)_2$), 1.51 (s, 1H, N_2-CH, 1.14 (dd, 24 H, $^3J_{H-H}$ = 6.9Hz, Imidazol-CH(C*H*$_3)_2$), 0.92 (d, 12H, $^3J_{H-H}$ = 6.7 Hz, CH(C*H*$_3)_2$), 0.67(d, 12H, $^3J_{H-H}$ = 6.8 Hz, CH(C*H*$_3)_2$).

^{13}C-NMR (100 MHz, THF-d_8, 300 K): δ[ppm]= 148.1 (*C*-imidazole), 146.8 (NCH) 146.1 (NCH), 138.5 (C-imidazole),133.0 (Ar-C), 129.7 (Ar-*C*), 129.0 (Ar-*C*), 126.1 (C-Ar), 126.1 (Ar-C), 124.9 (Ar-C), 124.8 (Ar-C), 122.6 (Ar-C), 30.2 (*C*-N_2), 30.1 (C*H*$(CH_3)_2$), 29.9 (*C*H-N_2), 24.8 (*C*H$(CH_3)_2$), 23.7 (CH(C*H*$_3)_2$), 23.2 (CH(C*H*$_3)_2$), 23.0 (CH(C*H*$_3)_2$), 21.6 (CH(C*H*$_3)_2$).

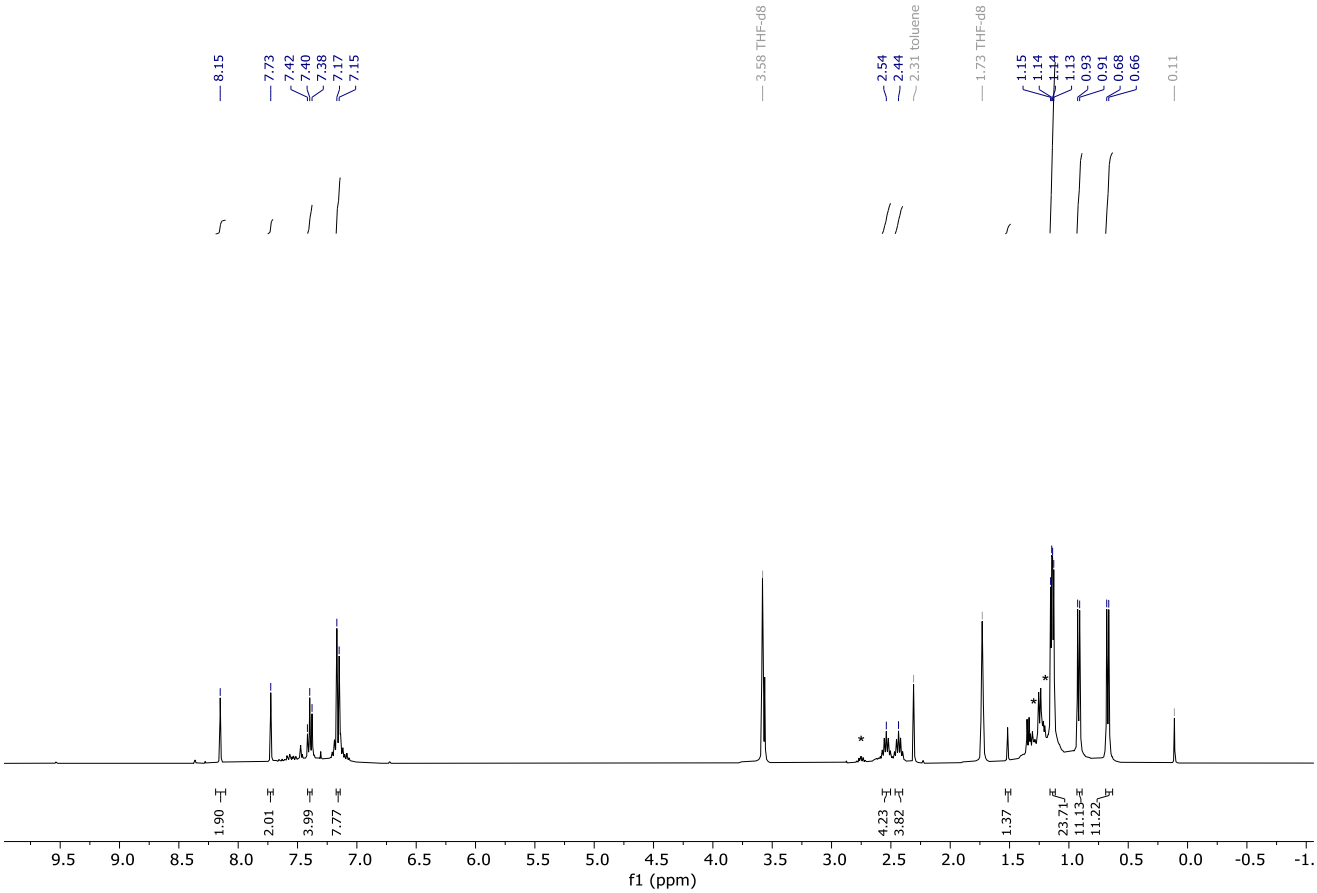

Figure S15: ^{1}H-NMR of the reaction of **A-1** with $GeCl_2$ dioxane in toluene measured in THF-d8. Formation of the non-fully characterized side product **1'.** Signals of **1** marked with *.

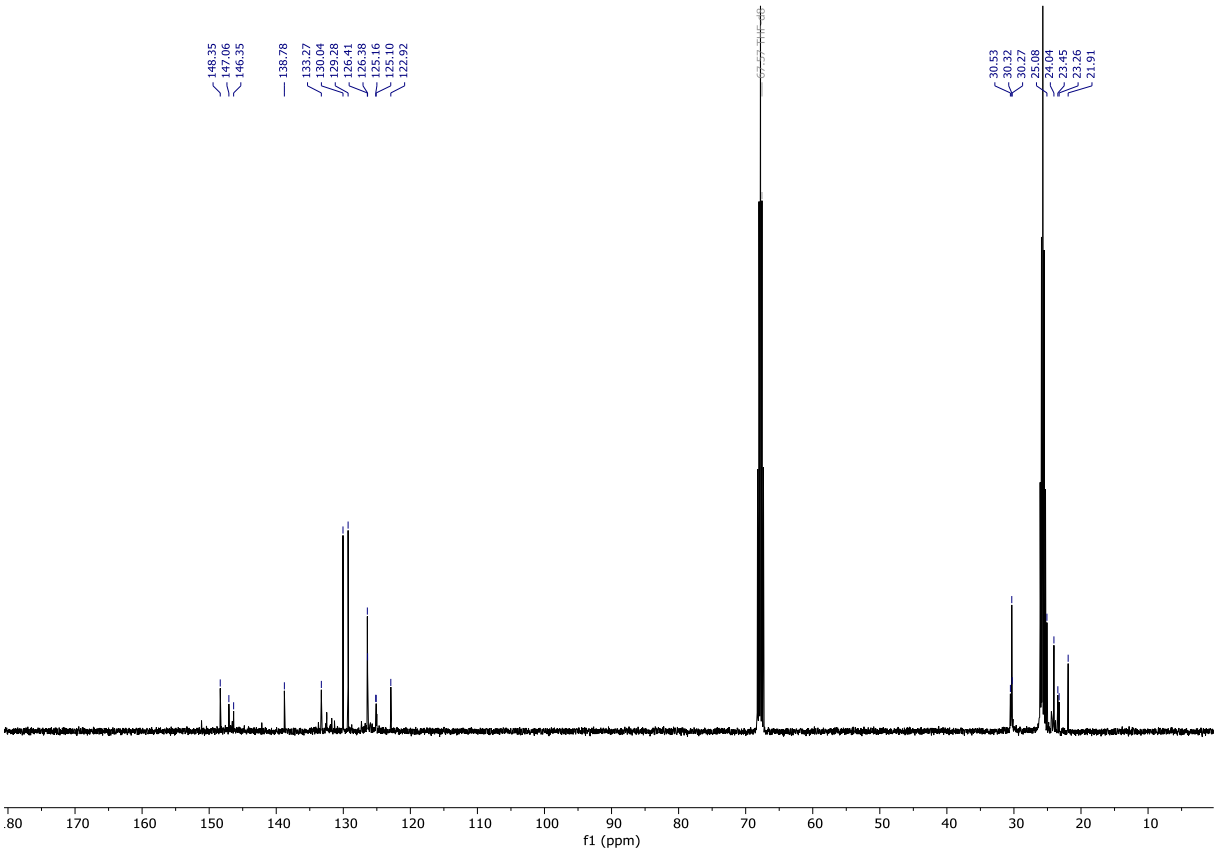

Figure S16: ^{13}C-NMR of the reaction of **A-1** with $GeCl_2$ dioxane in toluene measured in THF-d8. Formation of the non-fully characterized side product **1'.**

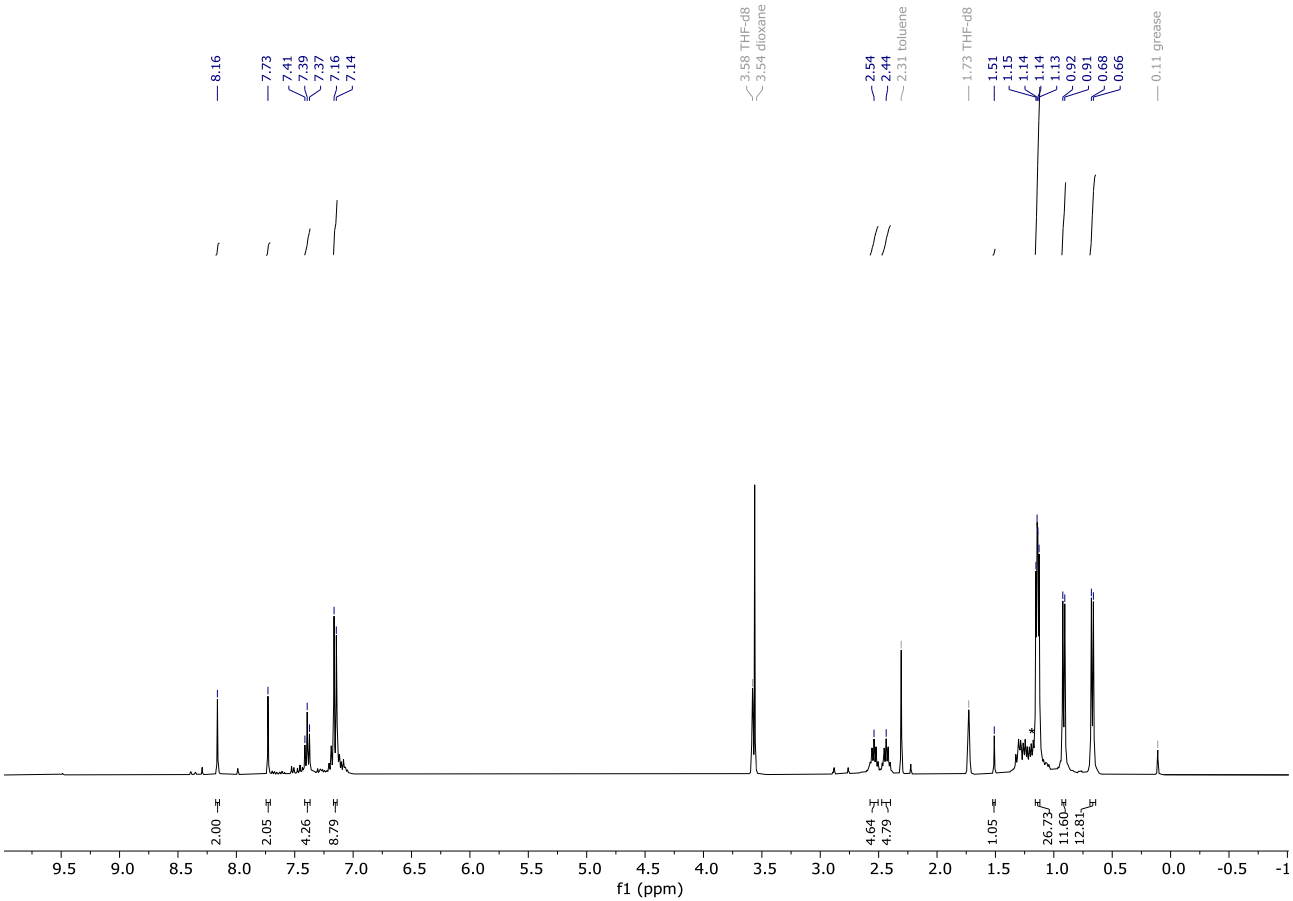

Figure S17: ^{1}H-NMR of the reaction of **A-1** with $SnCl_2$ dioxane in toluene measured in THF-d8. Formation of the non-fully characterized side product **2'.** Signals of **2** marked with *.

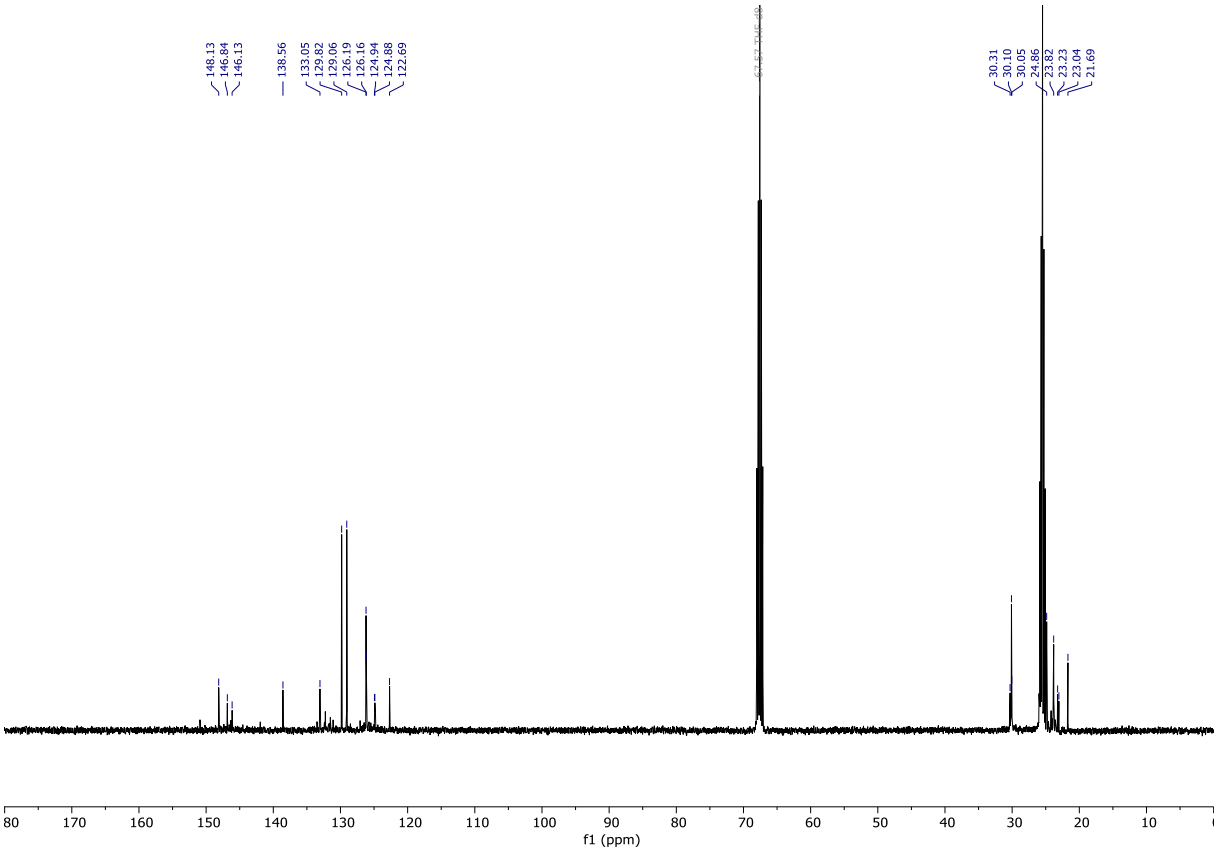

Figure S18: ^{13}C-NMR of the reaction of **A-1** with $SnCl_2$ dioxane in toluene measured in THF-d_8. Formation of the non-fully characterized side product **2'.**

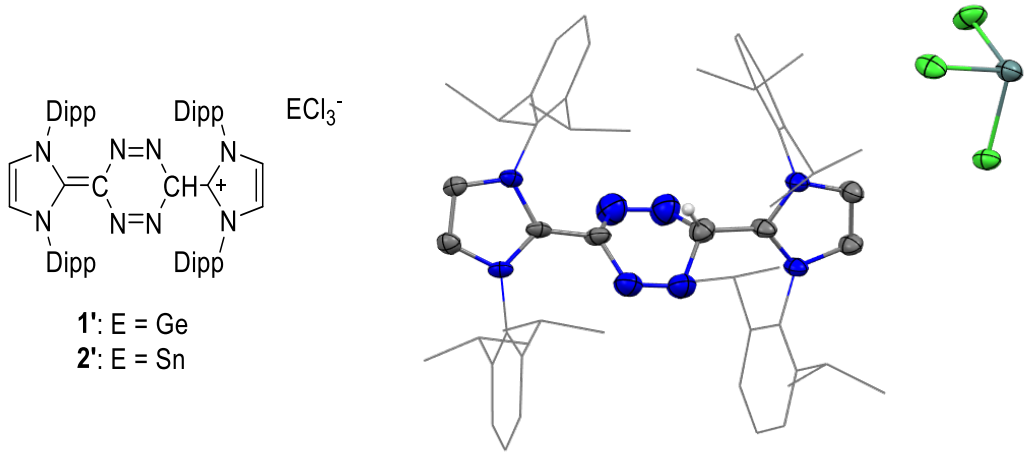

Figure S19: Structure and POV-Ray image of the side product **1'**. Data quality was not sufficient for publication but adequate to show the atom connectivity of the compound. Space group and asymmetric unit: Triclinic, P_i.

Synthesis of $KSi(TMS)_2Si(tolyl)_3$

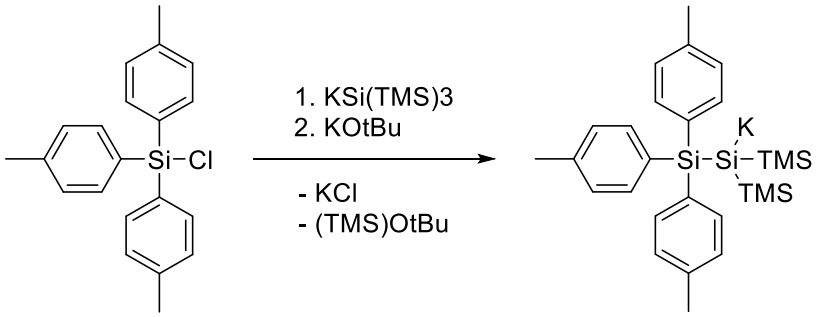

$Si(TMS)_3Si(tolyl)_3$ was synthesized according to the synthesis route established by Marschner for related compounds.[2] A solution of 2.00 g Cl-$Si(tolyl)_3$ (5.90 mmol, 1.00 eq) in 5.00 mL toluene was added dropwise to a solution of 1.70 g $KSiTMS_3$ (5.90 mmol, 1.00 eq) in toluene at -78°C. The solution was allowed to warm to room temperature and stired for 16 h. After filtration to remove KCl and removal of the solvent under reduced pressure $Si(TMS)_3Si(tolyl)_3$ remains as a beige solid which was used without further purification. 0.73 g KO^tBu (6.49 ,mol, 1.10 eq) were added to the silane and the mixture was dissolved in 20 mL THF. The solution turned yellow immediately and was allowed to stir for 16 h. After filtration and removal of the solvent the crude product was washed with 3 x 10 mL of cold hexane (approx. 0 °C). After drying in vacuum $KSi(TMS)_2Si(tolyl)_3$ was obtained as a yellow solid in 90 % total yield.

^{1}H-NMR (400 MHz, THF-d_8, 300 K): δ[ppm]= 7.47 (d, 6H, $^3J_{H-H}$ = 8.0 Hz, Ar-*H)*, 6.91 (d, 6H, $^3J_{H-H}$ = 8.1 Hz, Ar-*H*), 2.24 (s, 9H, tolyl-*Me*), -0.08 (s, 18 H, *TMS*).

^{13}C-NMR (100 MHz, THF-d_8, 300 K): δ[ppm]= 143.4 (Ar-*C*), 137.6 (Ar-*C*), 136.2 (Ar-*C*), 129.8 (Ar-*C*), 129.1 (Ar-*C*), 128.0 (Ar-*C*), 21.7 (tolyl-*Me*), 7.45 (*TMS*).

^{29}Si-NMR (100 MHz, THF-d_8, 300 K): δ[ppm]= -0.18 (*Si*$(tolyl)_3$), -6.59 (*TMS*), -189.8 (central *Si*).

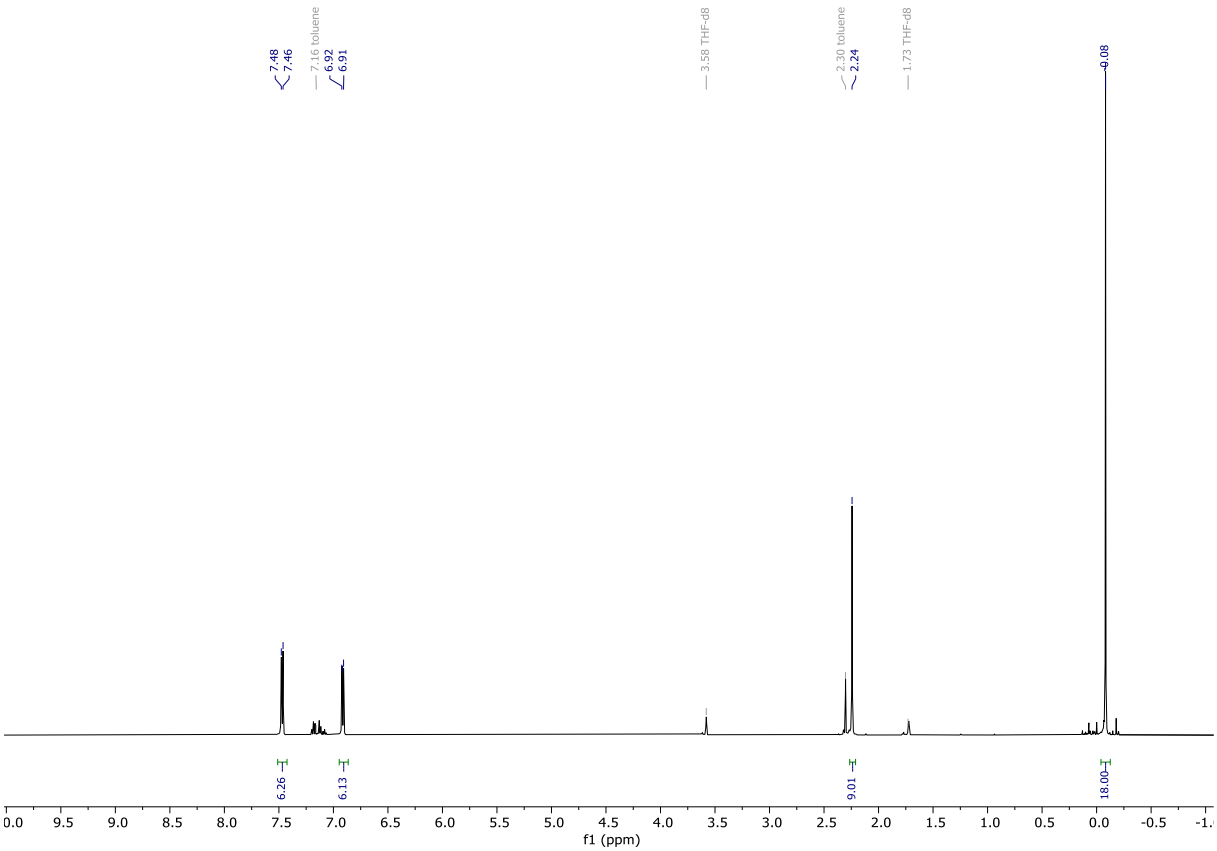

Figure S20: ^{1}H-NMR spectrum of KSi(TMS)$_2$Si(tolyl)$_3$ in THF-d$_8$

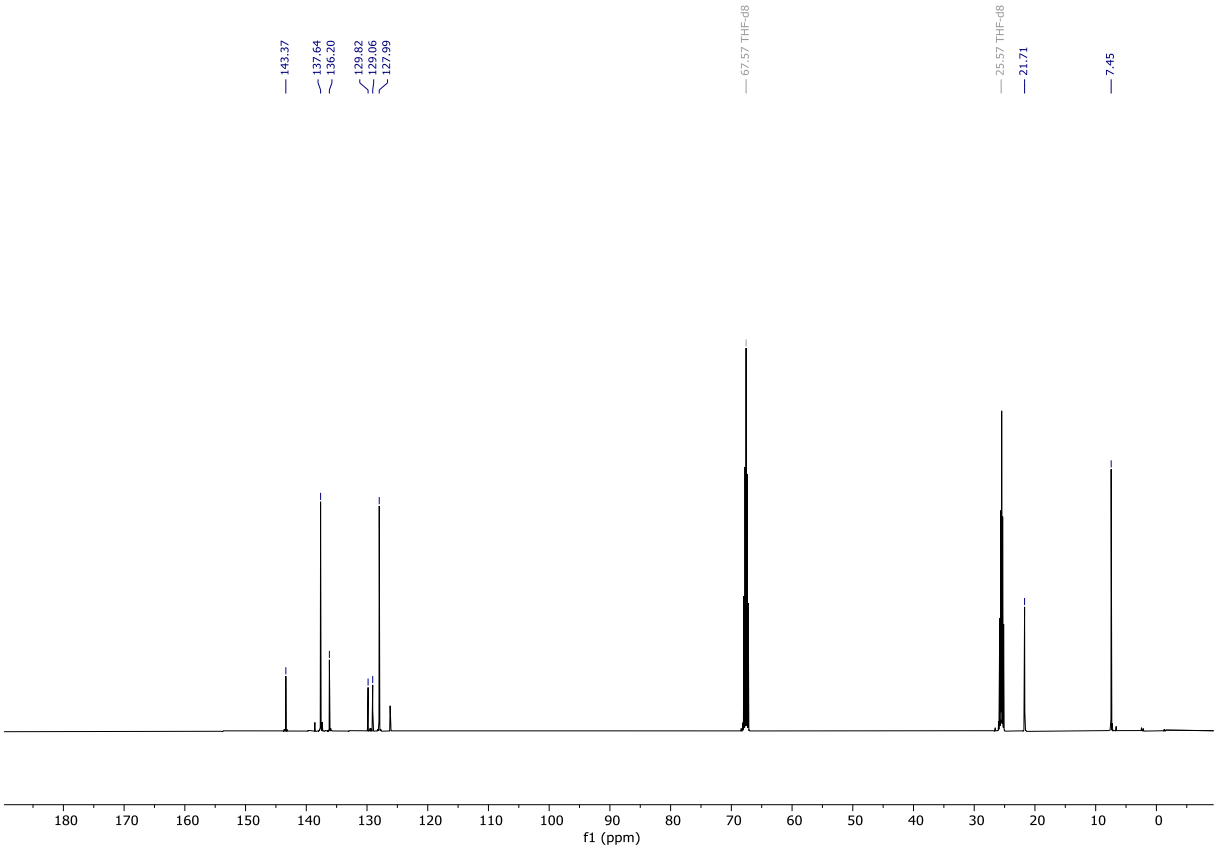

Figure S21: ^{13}C-NMR spectrum of KSi(TMS)$_2$Si(tolyl)$_3$ in THF-d$_8$

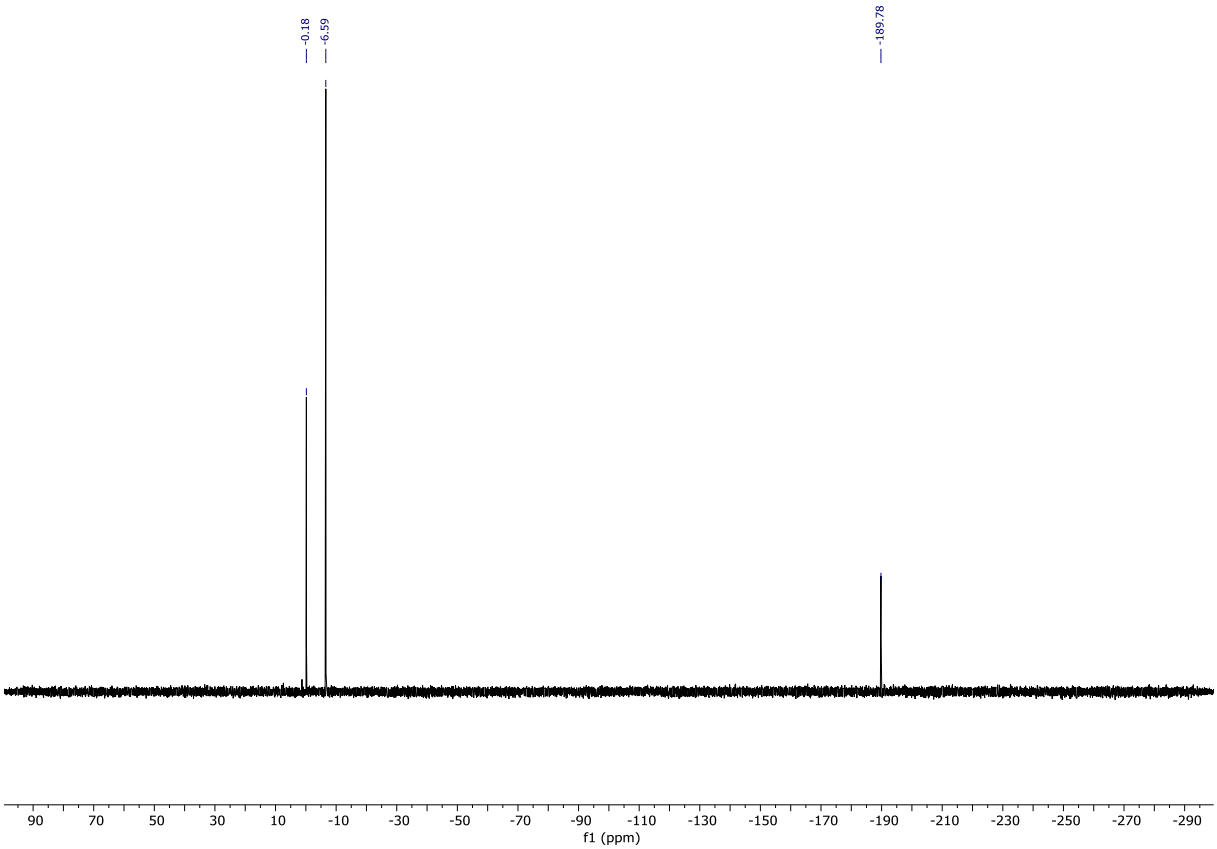

Figure S22: ^{29}Si-NMR spectrum of $KSi(TMS)_2Si(tolyl)_3$

Synthesis of bis-vinyl germylene $(NHO)_2$-N_2-Ge (3)

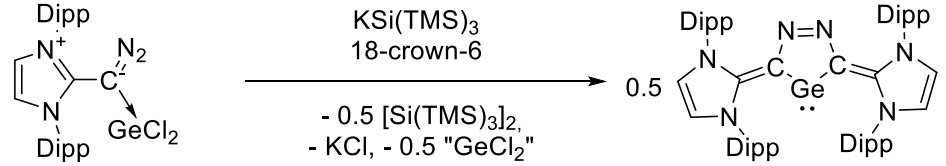

1 **3**

4 mL THF were added to 100mg ^{Dipp}NHO-$GeCl_2$ (0.18 mmol, 1.00 eq.), 4.62 mg 18-crown-6 (0.02 mmol, 0.10 eq.) and 50.12 mg $KSiTMS_3$ (0.18 mmol, 1.00 eq.) in a Schlenk flask and the solution was allowed to stir for 16 hours at room temperature. After evaporation of the solvent, the remaining solid was extracted with 3 x 7 mL pentane. The volume of the solution was reduced and placed in a freezer at -35°C to induce crystallization. Yellow to green germylene $(NHO)_2N_2$-Ge crystals could be collected in a total yield of 57% (45.10 mg, 0.05 eq.), containing approx. 10 mol% of crown ether.
A similar reaction procedure applies for the usage of the sterically modified silanides ($KSi(TMS)_2Si(^iPr)_3$ and $KSi(TMS)_2Si(tolyl)_3$) with a respective yield of 49% and 54%.

^{1}H NMR (400 MHz, C_6D_6, 300 K): δ[ppm]= 7.26 (t, 4H, $^3J_{H-H}$ = 7.7 Hz, Ar-*H*), 7.10 (d, 8H, $^3J_{H-H}$ = 7.7 Hz, Ar-*H*), 6.14 (s, 4H, NC*H*), 2.91 (hept, 8H, $^3J_{H-H}$ = 6.9 Hz, C*H*$(CH_3)_2$), 1.18 (d, 24H, $^3J_{H-H}$ = 6.9 Hz, CH(C*H*$_3)_2$), 1.05 (d, 24H, $^3J_{H-H}$ = 6.9 Hz, CH(C*H*$_3)_2$).

^{1}H NMR (400 MHz, THF-d8, 300 K): δ[ppm]= 7.69 (t, 4H, $^3J_{H-H}$ = 7.7 Hz, Ar-*H*), 6.98 (d, 8H, $^3J_{H-H}$ = 7.7 Hz, Ar-*H*), 6.79 (s, 4H, NC*H*), 2.73 (hept, 8H, $^3J_{H-H}$ = 6.9 Hz, C*H*$(CH_3)_2$), 1.08 (d, 24H, $^3J_{H-H}$ = 6.9 Hz, CH(C*H*$_3)_2$), 0.75 (d, 24H, $^3J_{H-H}$ = 6.9 Hz, CH(C*H*$_3)_2$).

^{13}C-NMR (100 MHz, C_6D_6, 300 K): δ[ppm]= 166.8 (C-N_2), 157.1 (*C*-imidazole), 146.4 (Ar-*C*), 136.9 (Ar-*C*), 129.1 (Ar-*C*), 124.2 (C-Ar), 119.0 (N*C*H), 29.2 (C*H*(CH_3)$_2$), 24.6 (CH(C*H*$_3$)$_2$), 23.4 (CH(C*H*$_3$)$_2$).

^{13}C-NMR (100 MHz, THF-d8, 300 K): δ[ppm]= 166.4 (C-N_2), 157.7 (*C*-imidazole), 147.1 (Ar-*C*), 137.8 (Ar-*C*), 129.2 (Ar-*C*), 124.4 (C-Ar), 120.2 (N*C*H), 29.8 (C*H*(CH_3)$_2$), 24.8 (CH(C*H*$_3$)$_2$), 23.7 (CH(C*H*$_3$)$_2$).

m.p.: 255 – 257 °C (decomposition)

IR (solid): $\tilde{\nu}$ [cm^{-1}] = 2960 (m), 2865 (m), 1464 (s), 1448 (s).

UV-Vis: λmax = 400 nm (ε = 318 L mol^{-1} cm^{-1})

NMR data of main side-products (disilanes):

[Si(TMS)$_3$]$_2$

^{1}H NMR (400 MHz, THF-d8, 300 K): δ[ppm]= 0.25 (s, 54 H, *TMS*)

^{13}C-NMR (100 MHz, THF-d8, 300 K): δ[ppm]= 3.17 (TMS).

^{29}Si-NMR (100 MHz, THF-d8, 300 K): δ[ppm]= -9.95 (TMS), -136.3 (cental Si).

[Si(TMS)$_2$Si(^{i}Pr)$_3$]$_2$

^{1}H NMR (400 MHz, THF-d8, 300 K): δ[ppm]= 1.19 (m, 6 H, SiC*H*(CH_3)$_2$), 1.16 (d, $^{3}J_{H-H}$ = 7.75 Hz, 36H, SiCH(C*H*$_3$)$_2$), 0.28 (s, 36 H, *TMS*).

^{13}C-NMR (100 MHz, THF-d8, 300 K): δ[ppm]= 20.8 (SiCH(*C*H_3)$_2$), 14.4 (Si*C*H(CH_3)$_2$), 0.99 (*TMS*).

^{29}Si-NMR (100 MHz, THF-d8, 300 K): δ[ppm]= -11.9 (*TMS*), -21.1 (*Si*(^{i}Pr)$_3$), -138.5 (central Si).

[Si(TMS)$_2$Si(tolyl)$_3$]$_2$

^{1}H NMR (400 MHz, THF-d8, 300 K): δ[ppm]= 7.38 (d, $^{3}J_{H-H}$ = 7.38 Hz, 12 H, *Ar-H*), 7.15 (d, $^{3}J_{H-H}$ = 7.38 Hz, 12 H, *Ar-H*), 2.33 (s, 18 H, tolyl-*Me*), 0.08 (s, 36 H, *TMS*).

^{13}C-NMR (100 MHz, THF-d8, 300 K): δ[ppm]= 140.4 (Ar-*C*), 137.3 (Ar-*C*), 132.3 (Ar-*C*), 129.7 (Ar-*C*), 21.8 (tolyl-*Me*), 0.32 (*TMS*).

^{29}Si-NMR (100 MHz, THF-d8, 300 K): δ[ppm]= -11.6 (*TMS*), -25.9 (*Si*(tolyl)$_3$), -132.5 (central Si).

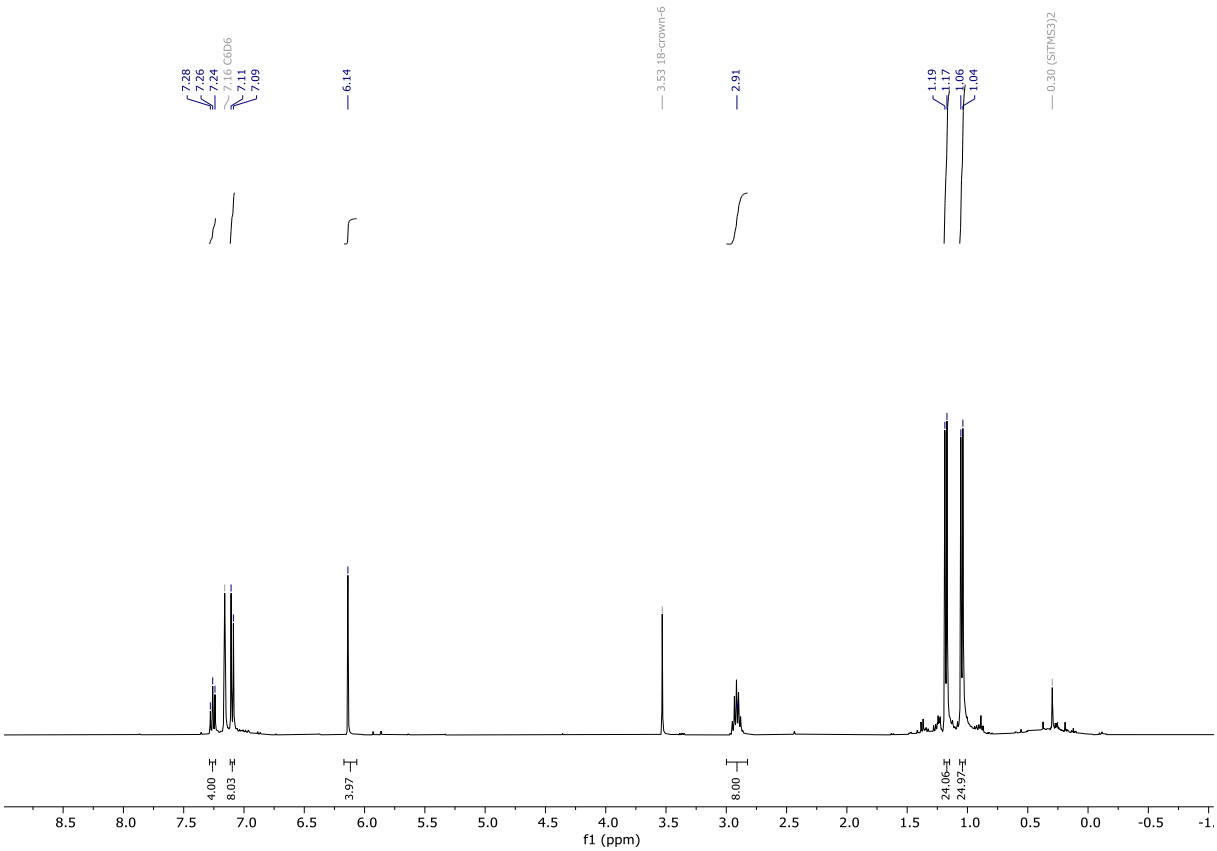

Figure S23: ^{1}H-NMR spectrum of bis-vinyl germylene 3 in C_6D_6

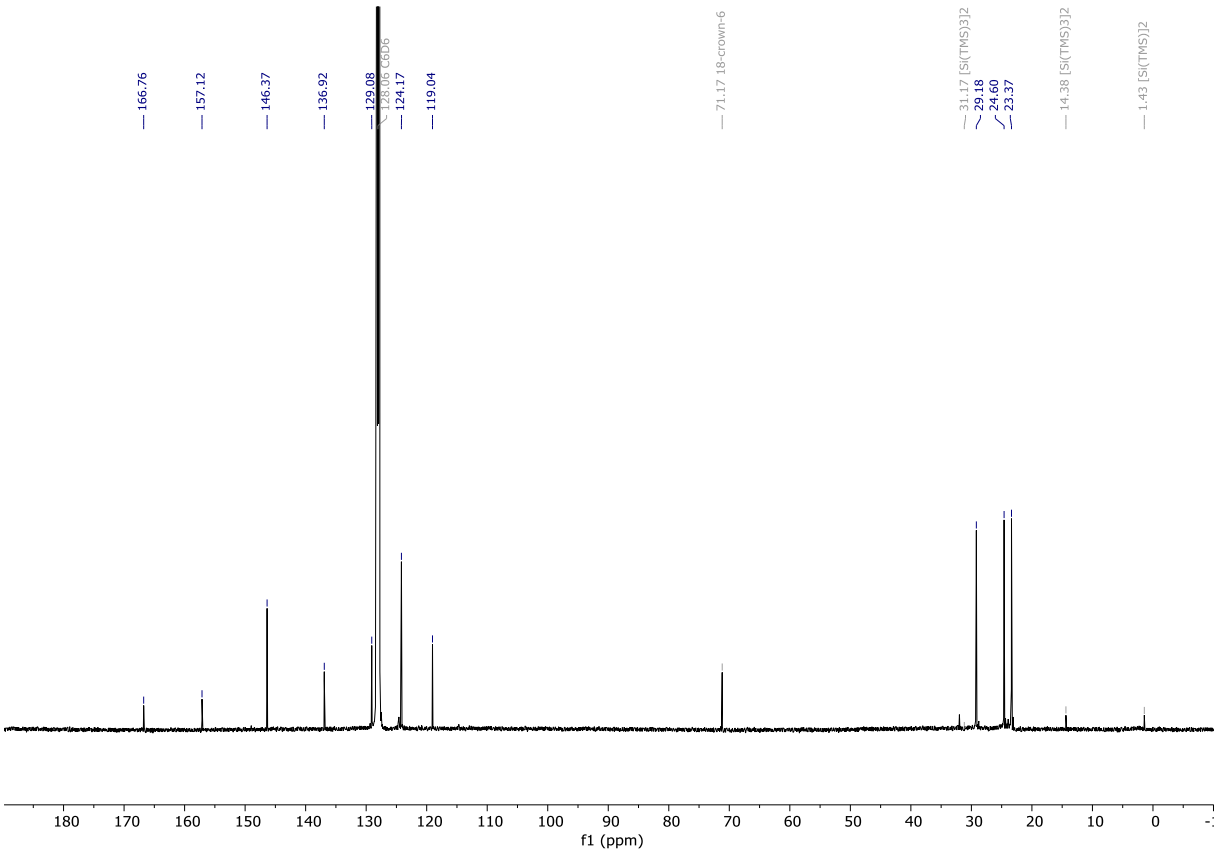

Figure S24: ^{13}C-NMR spectrum of bis-vinyl germylene **3** in C_6D_6.

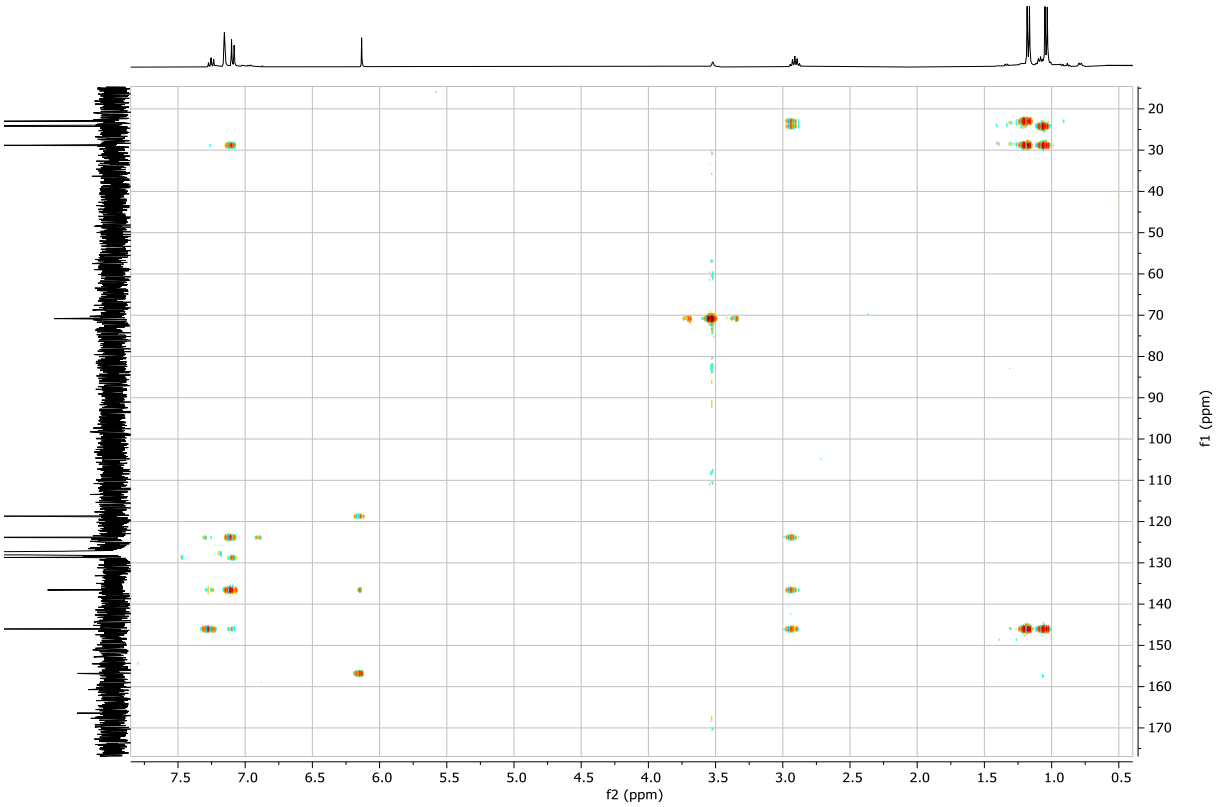

Figure S25: HMBC spectrum of bis-vinyl germylene 3 in C_6D_6.

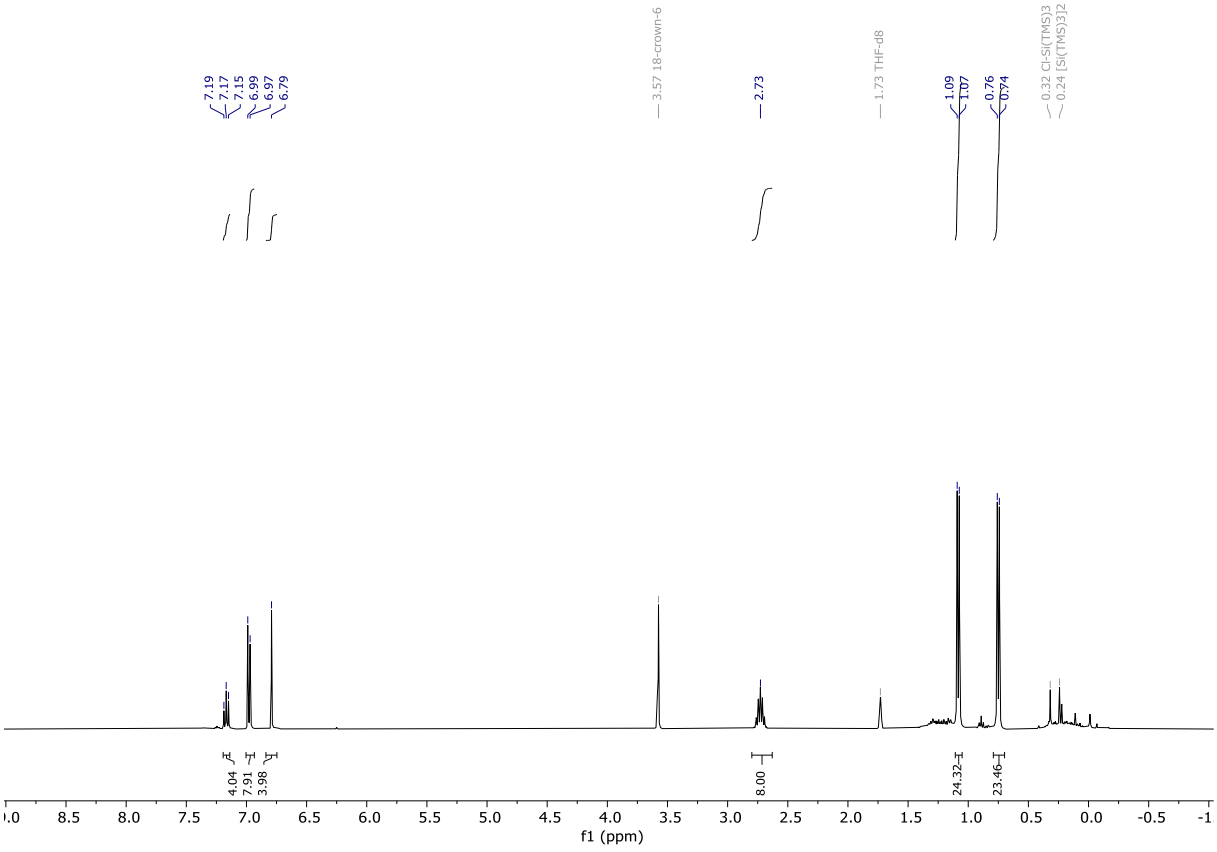

Figure S26: ^{1}H-NMR spectrum of bis-vinyl germylene **3** in THF-d_8.

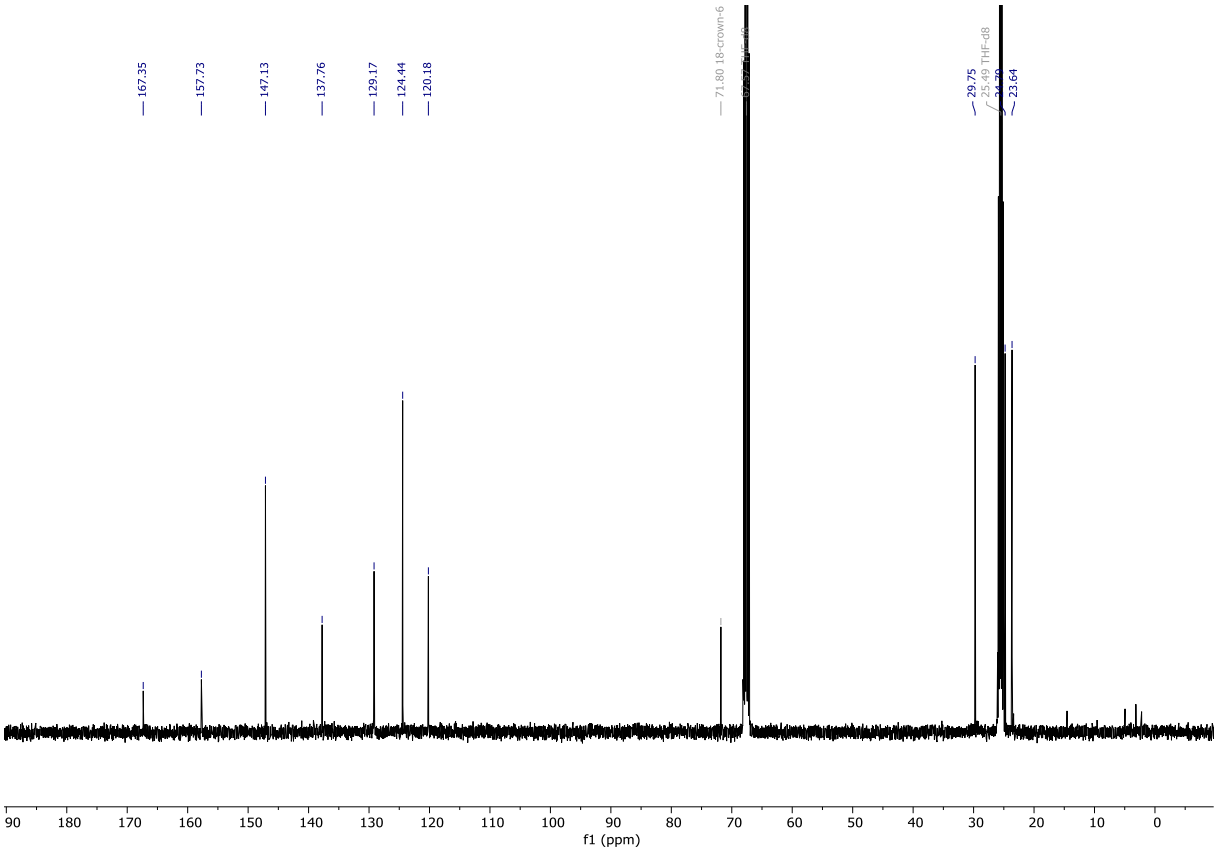

Figure S27: ^{13}C-NMR spectrum of bis-vinyl germylene **3** in THF-d_8.

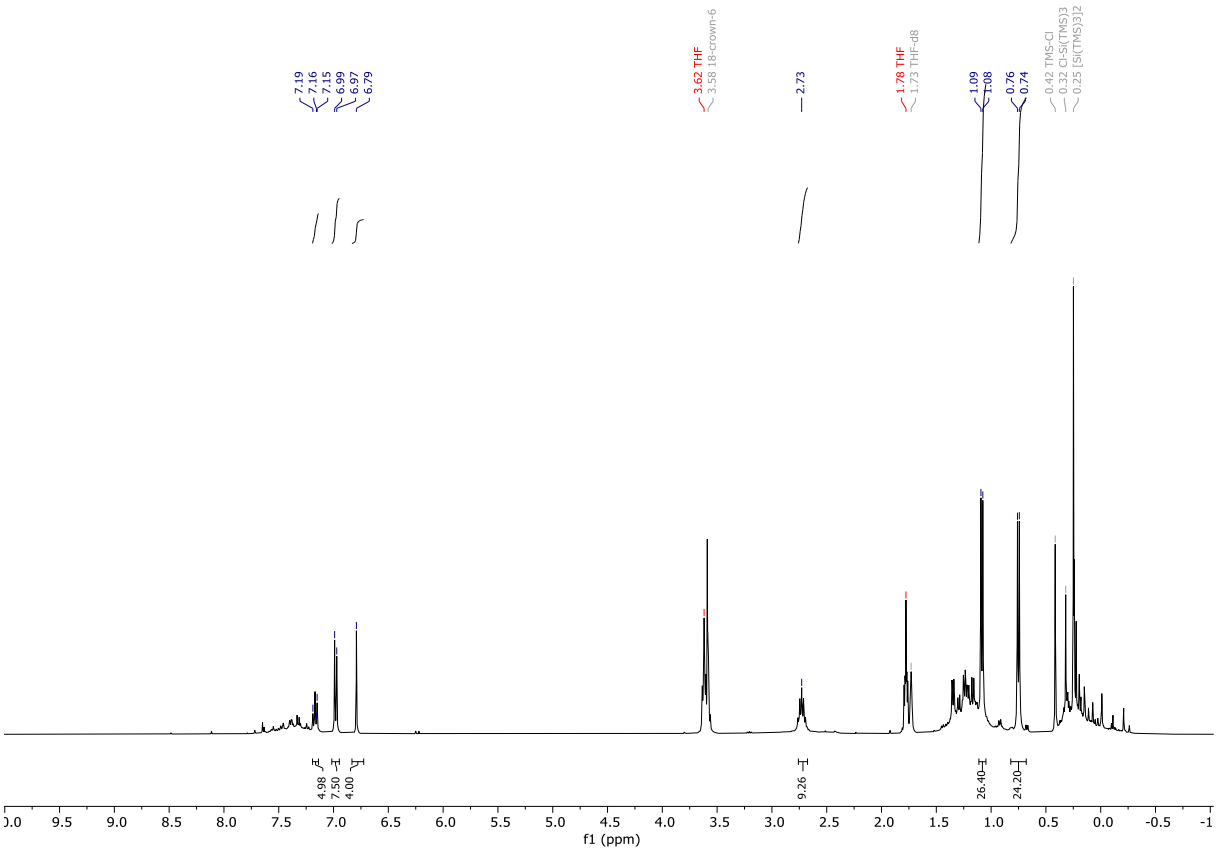

Figure S28: ^{1}H-NMR spectrum of the crude reaction mixture of **1** and $KSiTMS_3$ after 16h.

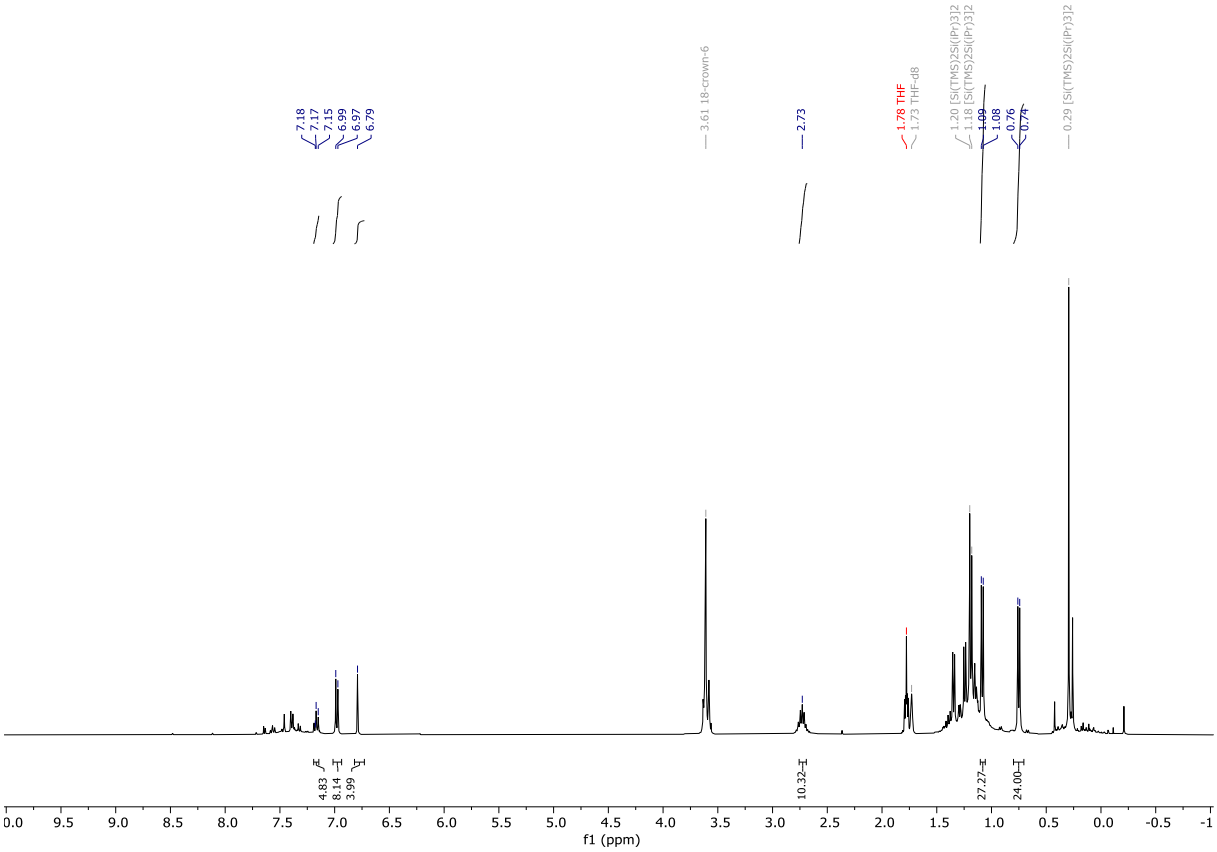

Figure S29: ^{1}H-NMR spectrum oft the reaction mixture of **1** and $KSi(TMS)_2Si(^{i}Pr)_3$ after 16 h in THF-d_8.

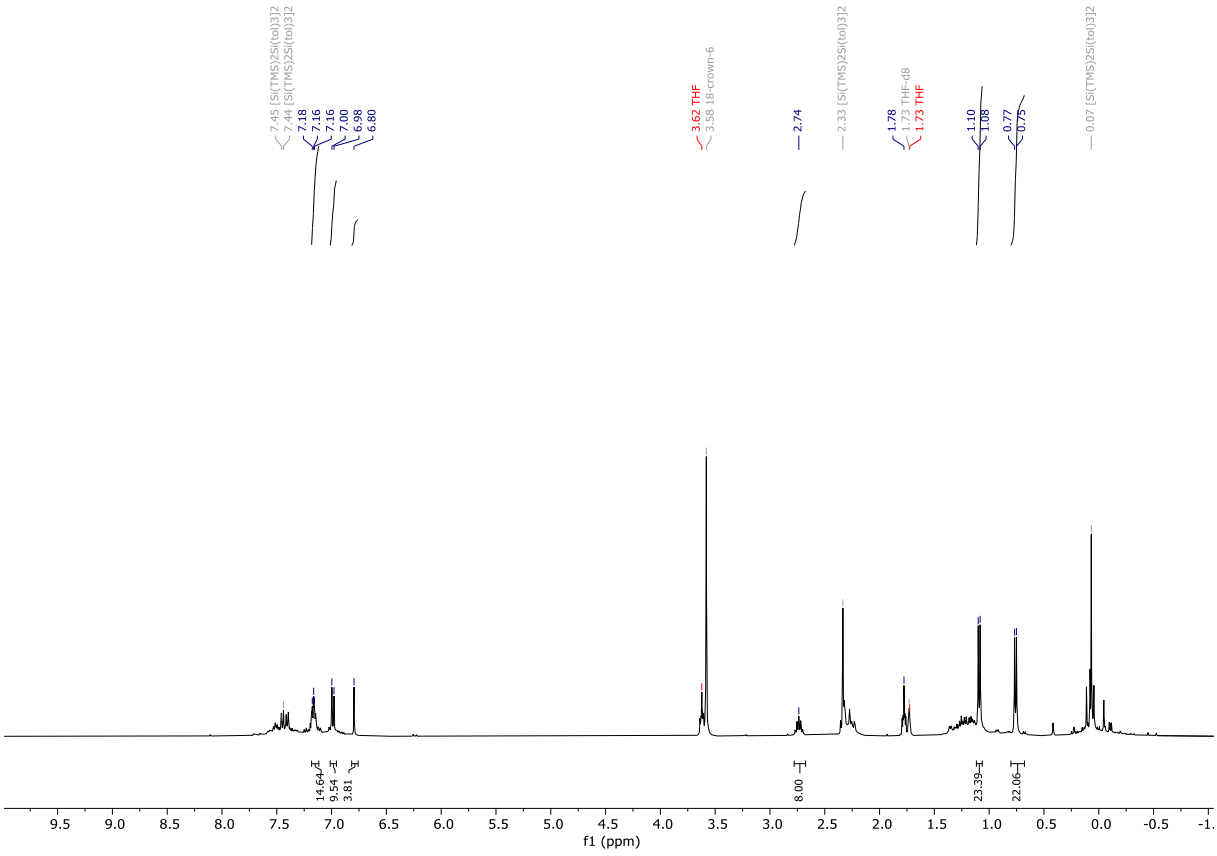

Figure S30: ^{1}H-NMR spectrum of the reaction mixture of **1** and $KSi(TMS)_2Si(tolyl)_3$ in after 16h in THF-d_8.

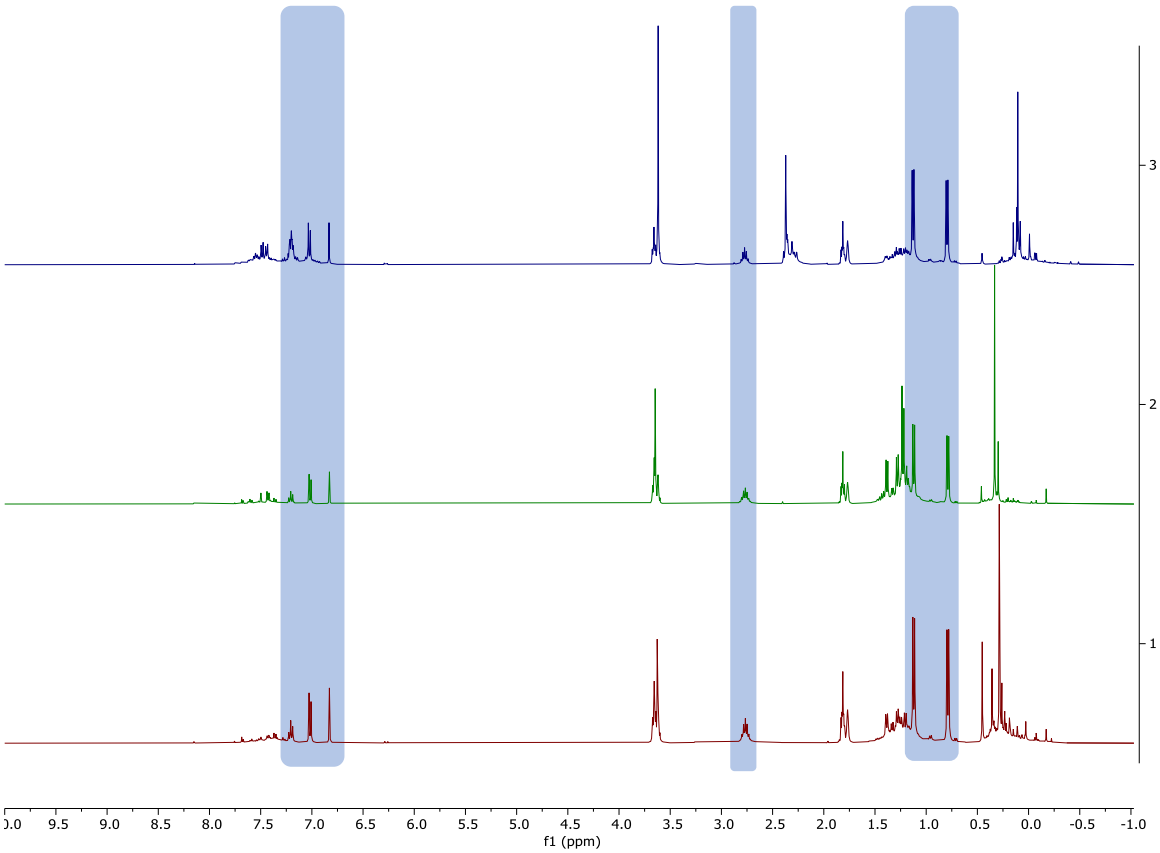

Figure S31: Overlay of Figure S28, S29 and S30: Formation of the same main product **3** in all reactions.

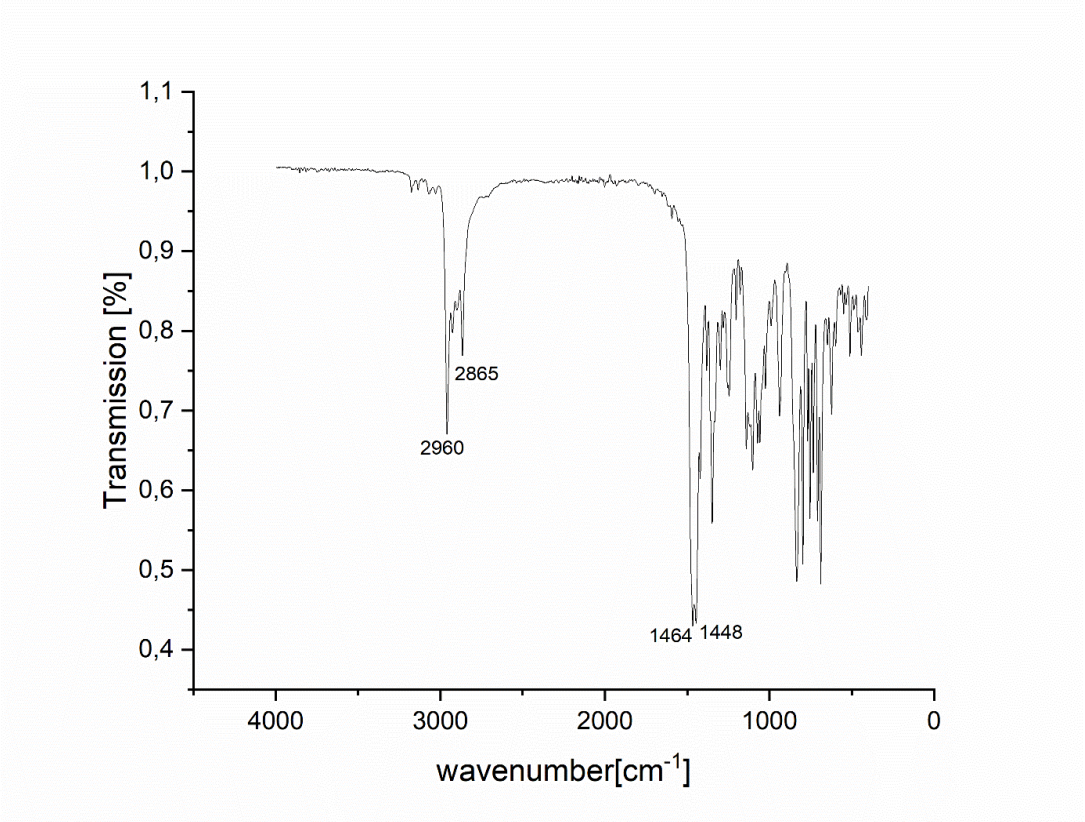

Figure S32: IR spectrum (solid) of bis-vinyl germylene **3**.

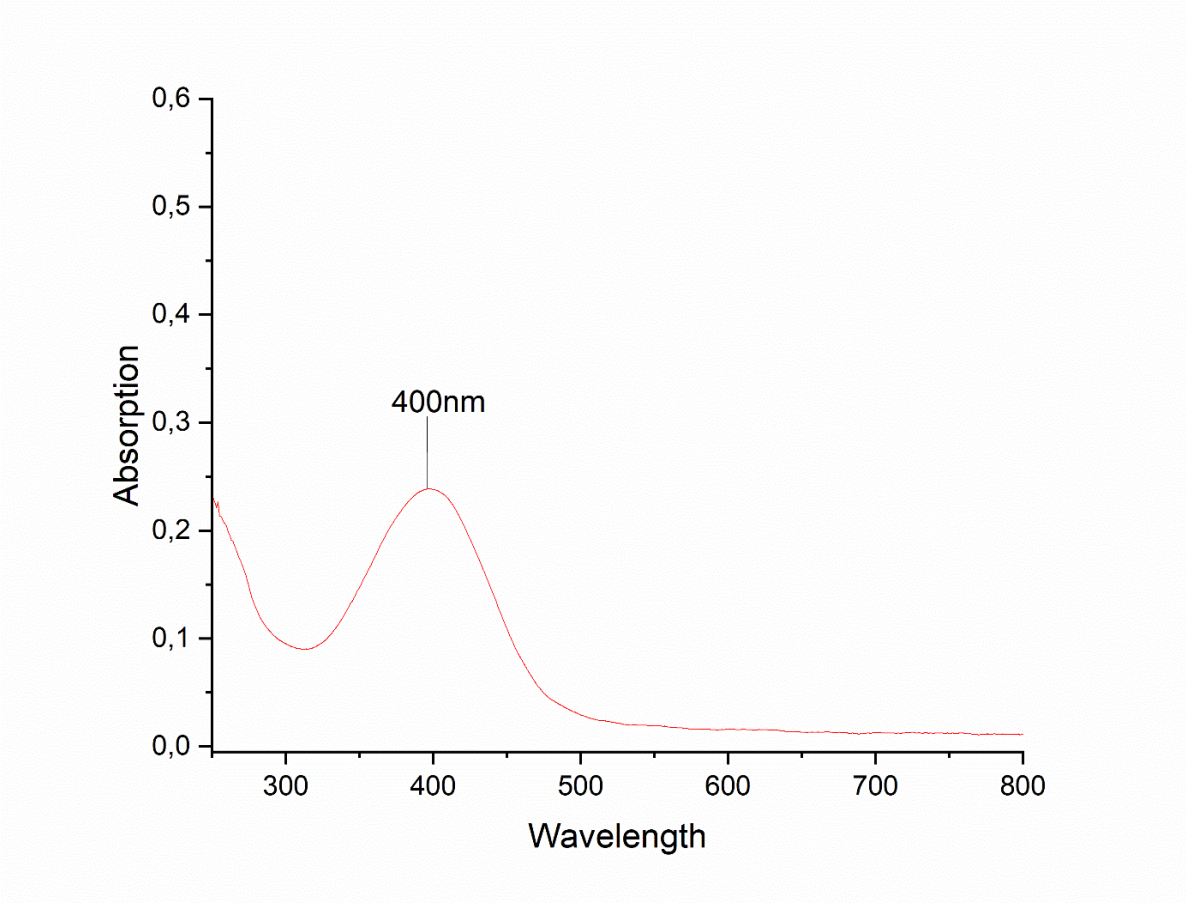

Figure S33: UV-Vis spectrum (hexane solution) of bis-vinyl germylene **3**; c = 0.75 mM

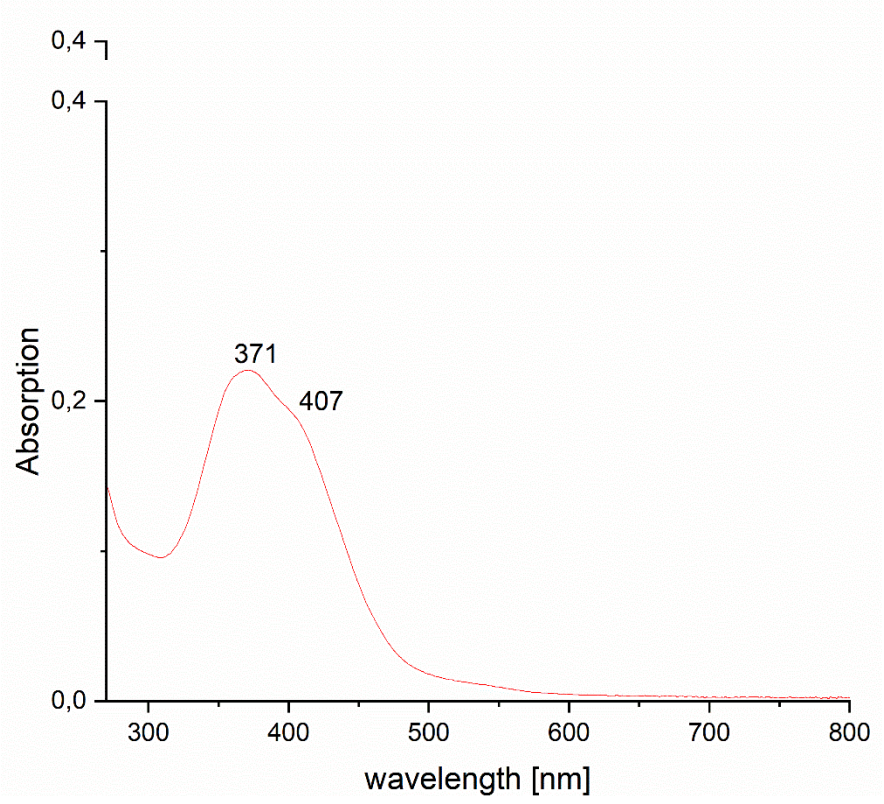

Figure S34: UV-Vis spectrum (hexane solution) of bis-vinyl germylene **3**; c = 0.5 mM

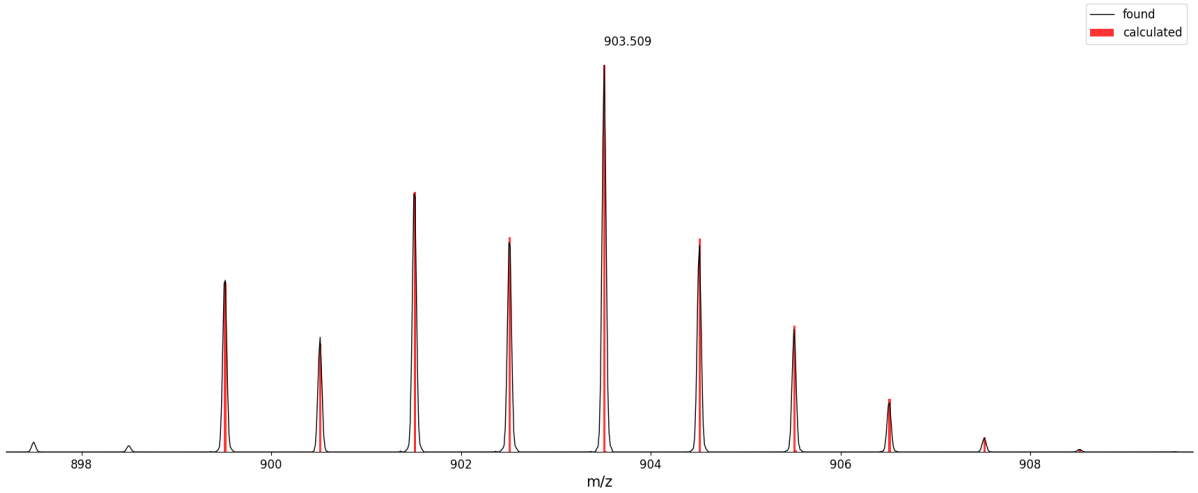

Figure S35: LIFDI-MS of bis-vinyl germylene **3**.

2. Single Crystal X-ray structure determination

Single crystal diffraction data were recorded on a Bruker instrument equipped with a Helios optic monochromator, a Mo IMS microsource (λ = 0.71073 Å) or a TXS rotating anode with Photon area detectors. The data collection was performed using the APEX III software package[5] on single crystals coated with Fomblin®Y as perfluorinated ether. The single crystals were picked on a MiTiGen MicroMount microsampler, transferred to the diffractometer and measured frozen under a stream of cold nitrogen (100 K). A matrix scan was used to determine the initial lattice parameters. Reflections were merged and corrected for Lorenz and polarization effects, scan speed, and background using SAINT.[6] Absorption corrections, including odd and even ordered spherical harmonics were performed using SADABS.[6] Space group assignments were based upon systematic absences, E statistics, and successful refinement of the structures. Structures were solved by direct methods with the aid of successive difference Fourier maps and were refined against all data using the APEX III software in conjunction with SHELXL-2014[7] and SHELXLE[9] or Olex2 software.[9] H atoms were placed in calculated positions and refined using a riding model, with methylene and aromatic C–H distances of 0.99 and 0.95 Å, respectively, and Uiso(H) = 1.2·Ueq(C). Non-hydrogen atoms were refined with anisotropic displacement parameters. Full-matrix least-squares refinements were carried out by minimizing $\Sigma w(Fo^2-Fc^2)^2$ with the SHELXL-97 weighting scheme.[9] Neutral atom scattering factors for all atoms and anomalous dispersion corrections for the non-hydrogen atoms were taken from International Tables for Crystallography.[10] The images of the crystal structures were generated by Mercury.[11] The CCDC numbers CCDC-2301470, CCDC-2301471 and CCDC-2301472 contain the supplementary crystallographic data for the structures **1**, **2** and **3**. These data can be obtained free of charge from the Cambridge Crystallographic Data Centre via https://www.ccdc.cam.ac.uk/structures/.

	compound_1	**compound_2**	**compound_3**
CCDC Number	2301470	2301471	2301472
Crystal data			
Chemical formula	$C_{28}H_{36}Cl_2GeN_4$	$2(C_{28}H_{36}Cl_2N_4Sn)\cdot C_4H_4O\cdot 2(C_4H_8O)$	$C_{56}H_{72}GeN_6$
M_r	572.10	1448.72	901.78
Crystal system, space group	Monoclinic, $P2_1/c$	Monoclinic, Cc	Monoclinic, $C2/c$
Temperature (K)	100	100	100
a, b, c (Å)	9.1689 (6), 16.1850 (9), 22.5667 (13)	31.096 (2), 12.7331 (8), 18.1401 (11)	39.420 (2), 12.4890 (8), 22.5821 (13)
α, β, γ (°)	90, 94.330 (3), 90	90, 94.162 (3), 90	90, 111.047 (4), 90
V (Å^3)	3339.3 (3)	7163.6 (8)	10375.7 (11)
Z	4	4	8
F(000)	1192	2992	3856
Radiation type	Mo $K\alpha$	Mo $K\alpha$	Mo $K\alpha$
No. of reflections for cell measurement	9842	9327	9253
θ range (°) for cell measurement	2.6–37.8	2.6–25.7	2.4–25.7
μ (mm^{-1})	1.10	0.90	0.63
Crystal shape	Block	Needle	Fragment
Colour	Yellow	Yellow	Yellow
Crystal size (mm)	0.06 × 0.03 × 0.02	0.66 × 0.37 × 0.23	0.29 × 0.27 × 0.18
Data collection			
Diffractometer	Bruker Photon CMOS	Bruker Photon CMOS	Bruker Photon CMOS
Radiation source	TXS rotating anode	IMS microsource	IMS microsource
Detector resolution (p mm^{-1})	16	16	16
Scan method	phi– and ω–rotation scans	phi– and ω–rotation scans	phi– and ω–rotation scans
Absorption correction	Multi-scan	Multi-scan	Multi-scan
T_{min}, T_{max}	0.6630, 0.7492	0.620, 0.745	0.666, 0.745
No. of measured, independent and observed [$I > 2\sigma(I)$] reflections	700304, 29697, 21195	175354, 13617, 13537	239774, 9922, 8872
R_{int}	0.108	0.050	0.065
θ values (°)	θ_{max} = 25.2, θ_{min} = 2.2	θ_{max} = 25.71, θ_{min} = 2.04	θ_{max} = 25.78, θ_{min} = 1.87
$(\sin\theta/\lambda)_{max}$ (Å^{-1})	1.022	0.610	0.612
Range of h, k, l	h = -18→18, k = -32→33, l = -45→45	h = -37→37, k = -15→15, l = -22→22	h = -48→48, k = -15→15, l = -27→27
Refinement			
Refinement on	F^2	F^2	F^2
$R[F^2 > 2\sigma(F^2)]$, $wR(F^2)$, S	0.041, 0.120, 1.03	0.017, 0.044, 1.05	0.036, 0.088, 1.03
No. of reflections	29697	13617	9922
No. of parameters	324	822	584
H-atom treatment	H-atom parameters constrained	H-atoms treated by a mixture of independent and constrained	H-atom parameters constrained

		refinement	
Weighting scheme	$w = 1/[\sigma^2(F_o^2) + (0.0561P)^2 + 0.6647P]$ where $P = (F_o^2 + 2F_c^2)/3$	$w = 1/[\sigma^2(F_o^2) + (0.0204P)^2 + 4.7665P]$ where $P = (F_o^2 + 2F_c^2)/3$	$w = 1/[\sigma^2(F_o^2) + (0.0374P)^2 + 18.3191P]$ where $P = (F_o^2 + 2F_c^2)/3$
$\Delta\rho_{max}$, $\Delta\rho_{min}$ (e Å^{-3})	0.86, -1.17	0.43, -0.35	0.43, -0.78
Absolute structure	–	Flack (1983)	–
Absolute structure parameter	–	0.367 (10)	–

3. Computational details

Calculations were carried out using Gaussian 16.8 software.[13] The geometry of all compounds were optimized at the B3LYP[14] level of theory. For compound **1,** a 6-311+G(d,p) basis set[15] was used for all atoms. For compound **2,** the same basis set was used, except for tin, where an augmented basis set has been used that previously showed reliable predictions for tin compounds.[16] For compound **3,** the 6-311+G(d,p) basis set was used for germanium. A basis set of 6-31G(d,p) was used for all other atoms. Analytical frequency calculations verified the optimized geometries as minima or transition states. Cartesian coordinates of all optimized geometries are in a separate file (compounds1-3.xyz) in .xyz format.

Table 1: Energies (E^h) (E – electronic energy; H – total enthalpy; G – Gibbs energy) of the calculated compounds.

Compound	E	H	G
1	-4305.63991183	-4305.012412	-4305.124694
2	-8249.61703525	-8248.989714	-8249.103181
3	-4583.07671725	-4581.841017	-4582.008131

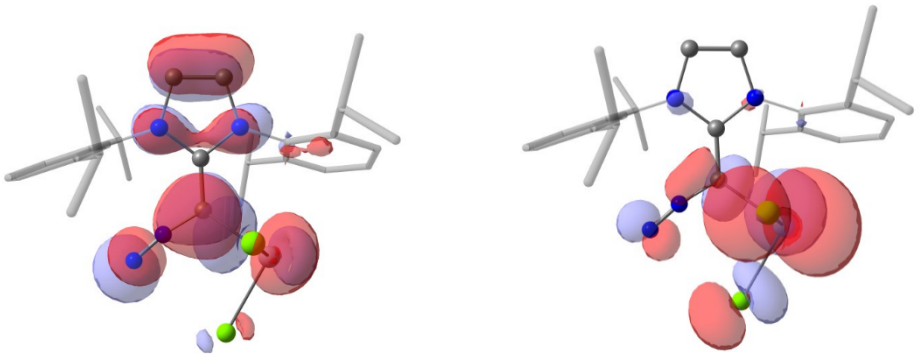

Figure S36: Selected Molecular orbitals of compound **1**: a) HOMO-1, b) HOMO

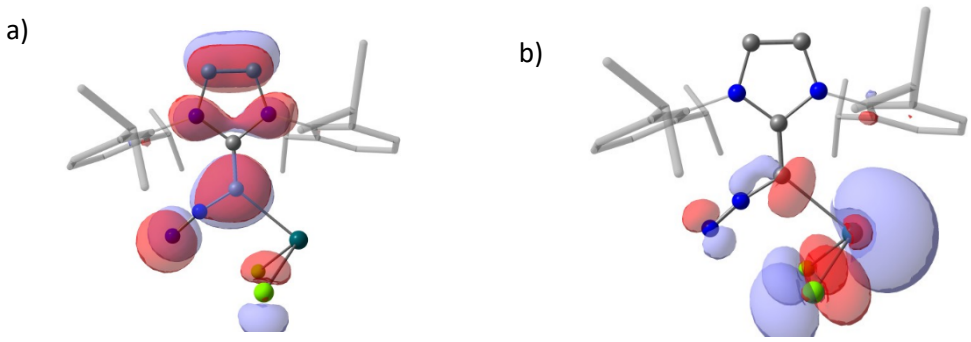

Figure S37: Selected Molecular orbitals of compound **2**: a) HOMO-1, b) HOMO

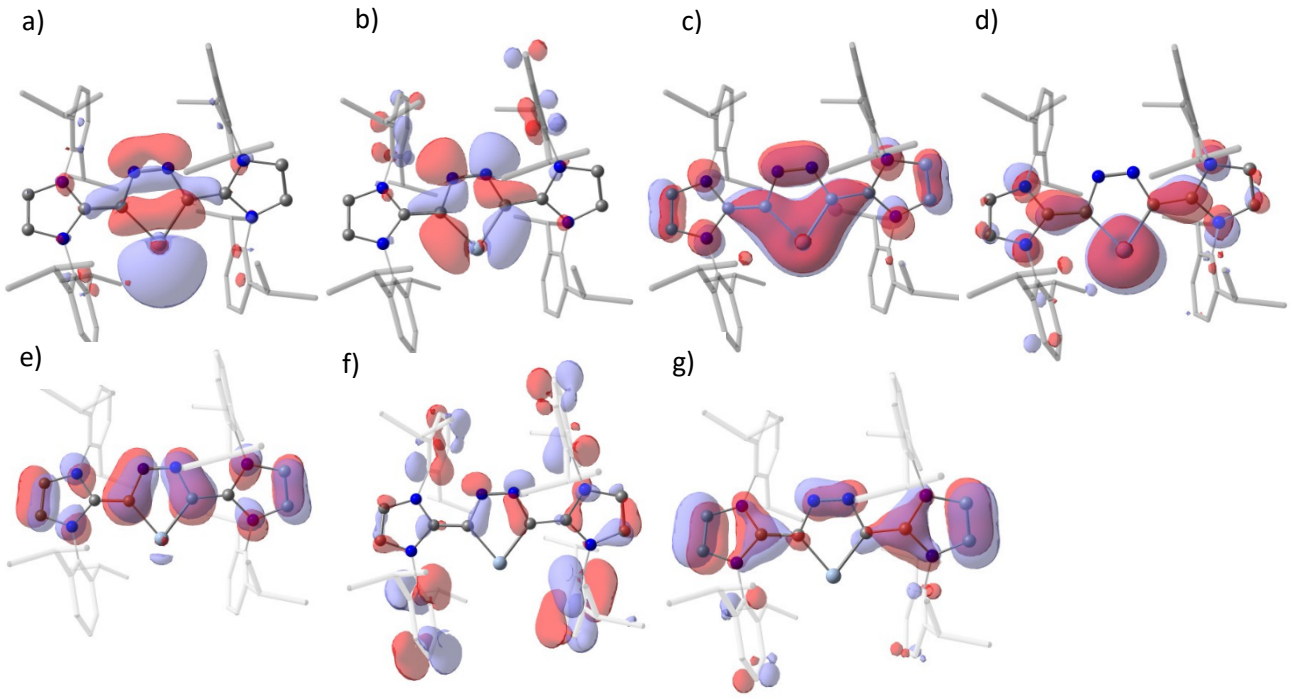

Figure S38: Selected Molecular orbitals of compound **3**: a) HOMO-2, b) HOMO-1, c) HOMO, d) LUMO, e) HOMO-3, f) HOMO-11, g) HOMO-12.

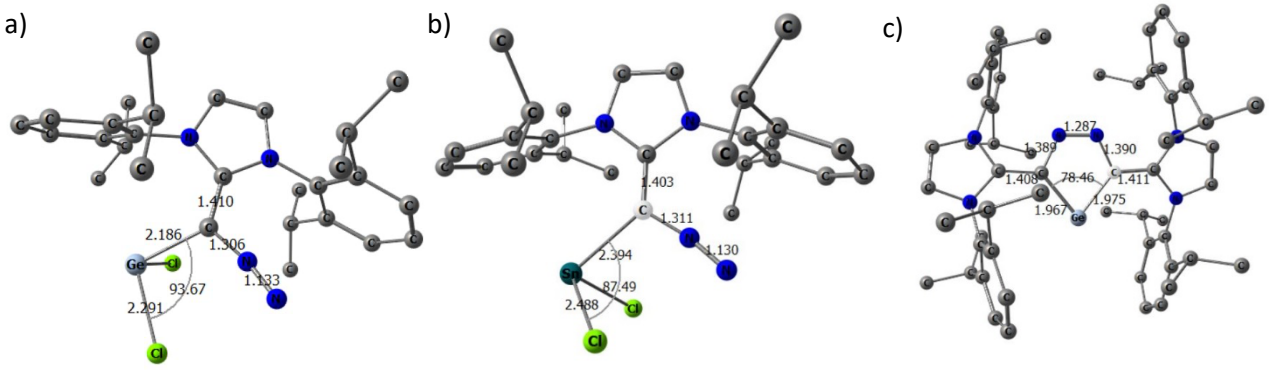

Figure S39: Visualization of the theoretical structures of a) **1**, b) **2,** and c) **3**. Hydrogens were omitted for clarity.

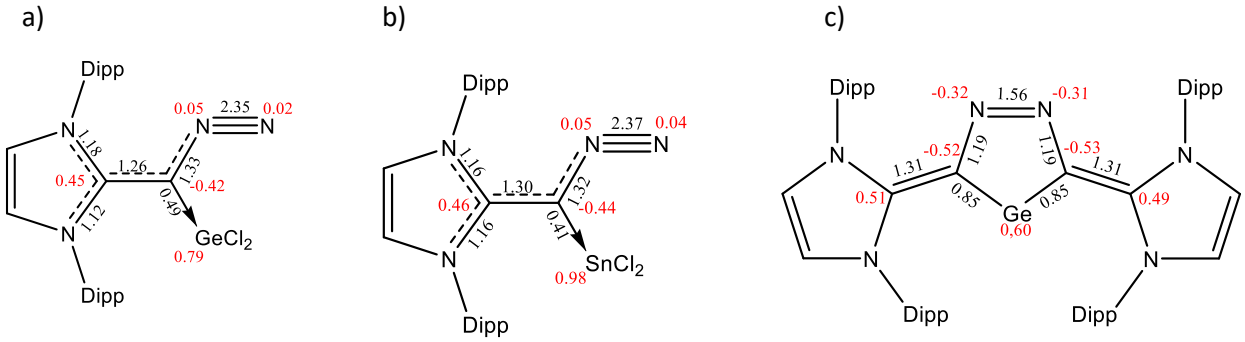

Figure S40: Selected Wiberg bond indices (black) and NPA charges (red) of a) **1**, b) **2** and c)**3**.

NBO analysis

Germanium adduct 1:

NBO analysis shows a lone pair (NBO 59, occupancy 1.98) on the terminal N59 atom and a σ (NBO 141) and two π bond orbitals (NBO 142 and 143) between N59 and N58. Between the central carbon atom C6 and N58 a single bond is present (NBO 81) while between C6 and the carbene carbon C4 a double bond is observable (NBO 78 and 79). Between C6 and Ge60 a polarized sp(C-Ge) bond (81.5%/18.5%) with an occupancy of 1.81 is shown in NBO 82. The germanium atom possesses a lone pair with 88.4% s character (NBO 60) and an empty p-type orbital (92.7%, NBO 150) with an occupancy of 0.44.

Second order perturbation theory analysis shows donor acceptor interactions (DAI) between the π bond of C4 and C6 towards the antibonding π N58-N59 bond of DAI = 42.5 kcal mol^{-1} (NBO 79 → NBO 225). Additional donor acceptor interaction into the second π N58 – N59 bond is observed from the C6-Ge60 bond (DAI = 22.6 kcal mol^{-1}, NBO 82 → NBO 226).

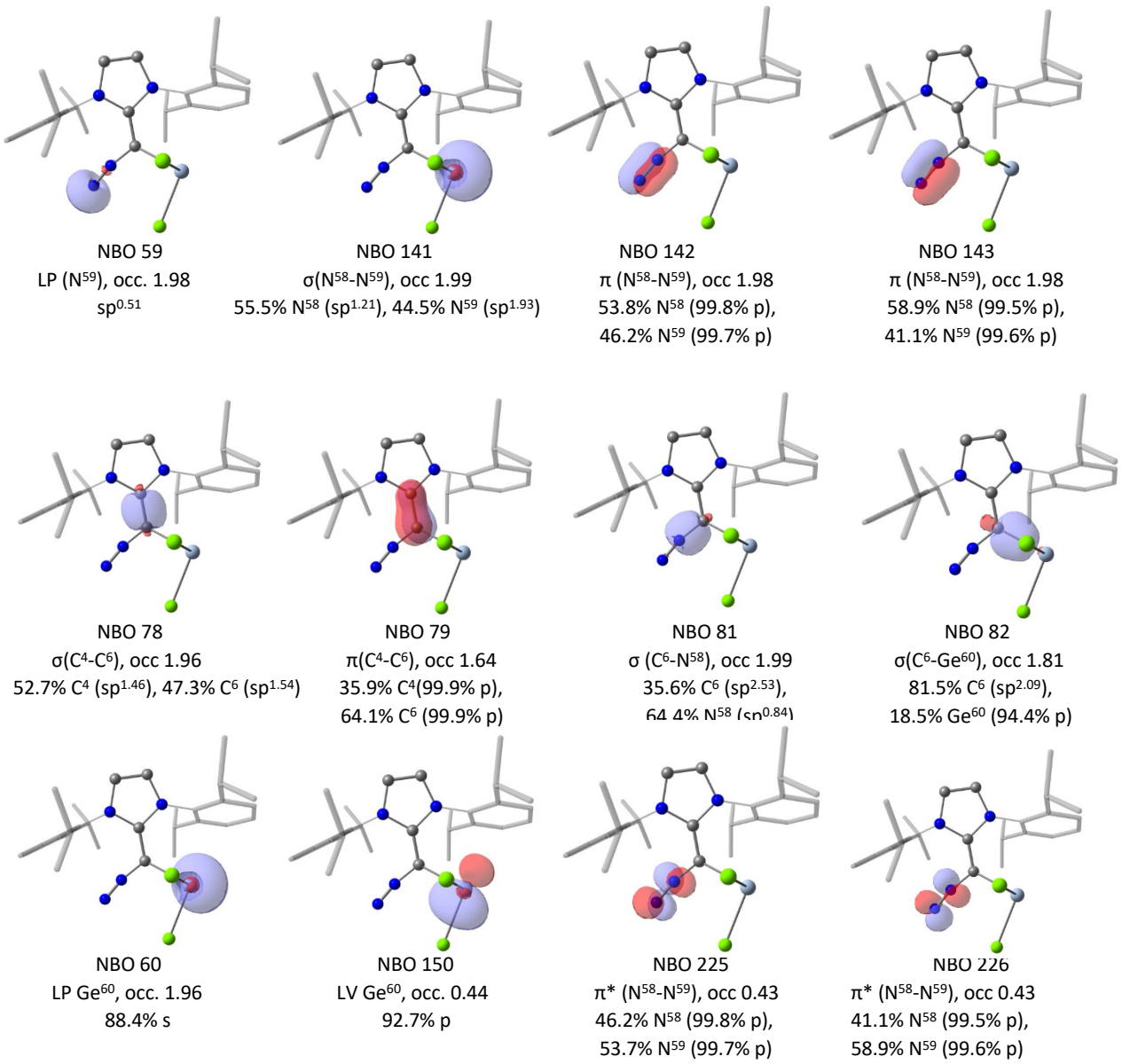

Figure S41: Selected NBO's of compound **1**.

Tin adduct 2:

A comparable structure to germanium complex **1** is observed. NBO analysis shows a lone pair (NBO 68, occupancy 1.97) on the terminal N20 atom and a σ (NBO 120) and two π bond orbitals (NBO 121 and 122) between N20 and N19. Between the central carbon atom C18 and N19 a single bond is present (NBO 118) while between C18 and the carbene carbon C4 a double bond is observable (NBO 87 and 88). Between C18 and Sn21 a polarized sp(C-Sn) bond (84.5%/15.5%) with an occupancy of 1.79 is shown in NBO 119. The tin atom possesses a lone pair with 88.1% s character (NBO 69) and an empty p-type orbital (92.3%, NBO 159) with an occupancy of 0.37.

Second order perturbation theory analysis shows donor acceptor interactions (DAI) between the π bond of C4 and C18 towards the antibonding π N19-N20 bond of DAI = 48.1 kcal mol^{-1} (NBO 88 → NBO 205). Additional donor acceptor interaction into the second π N19 – N20 bond is observed from the C18-Sn21 bond (DAI = 32.1 kcal mol^{-1}, NBO 119 → NBO 204).

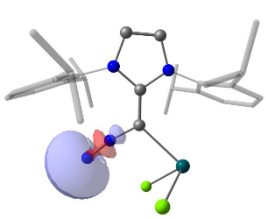

NBO 68
LP (N^{20}), occ. 1.97
$sp^{0.52}$

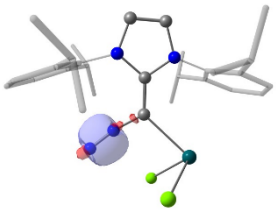

NBO 120
σ(N^{19}-N^{20}), occ 1.99
55.2% N^{19} ($sp^{1.22}$), 44.8% N^{20} ($sp^{1.89}$)

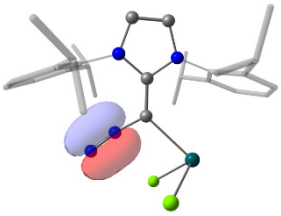

NBO 121
π (N^{19}-N^{20}), occ 1.99
59.1% N^{19} (99.3% p),
40.9% N^{20} (99.6% p)

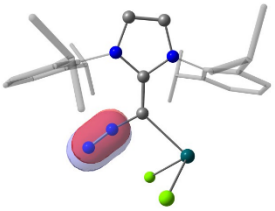

NBO 122
π (N^{19}-N^{20}), occ 1.98
54.2% N^{19} (99.9% p),
45.9% N^{20} (99.7% p)

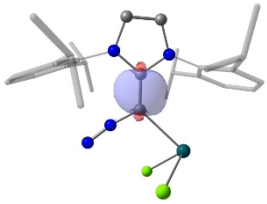

NBO 87
σ(C^4-C^{18}), occ 1.96
52.7% C^4 ($sp^{1.44}$), 47.3% C^{18} ($sp^{1.45}$)

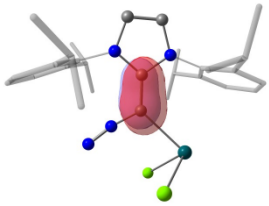

NBO 88
π(C^4-C^{18}), occ 1.67
37.5% C^4(99.9% p),
62.5% C^6 (99.9% p)

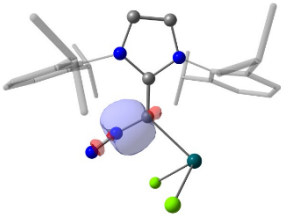

NBO 118
σ (C^{18}-N^{19}), occ 1.99
35.4% C^{18} ($sp^{2.56}$),
64.6% N^{19} ($sp^{0.84}$)

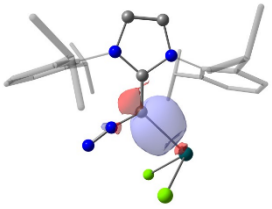

NBO 119
σ(C^{18}-Sn^{21}), occ 1.81
84.5% C^{18} ($sp^{2.19}$),
15.5% Sn^{21} (94.3% p)

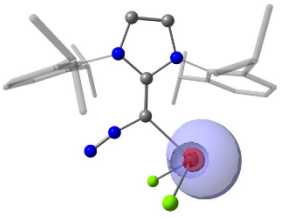

NBO 69
LP Sn^{21}, occ. 1.97
88.1% s

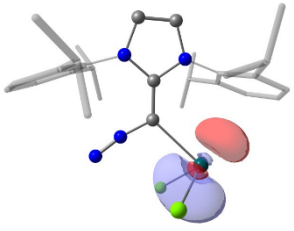

NBO 159
LV Sn^{21}, occ. 0.37
92.3% p

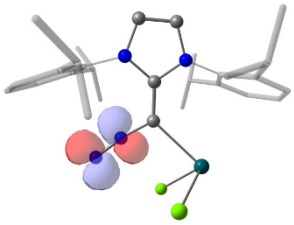

NBO 204
π (N^{19}-N^{20}), occ 0.20
40.9% N^{19} (99.3% p),
59.1% N^{20} (99.6% p)

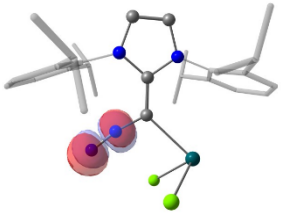

NBO 205
π (N^{19}-N^{20}), occ 0.43
45.9% N^{19} (99.9% p),
54.2% N^{20} (99.6% p)

Figure S42: Selected NBO's of compound **2**.

Germylene 3:

NBO analysis shows a lone pair with high s character (NBO 81, occupancy 1.97) on the germanium atom Ge68 and an empty p-orbital (NBO 242). A single bond between Ge 68 and the neighbouring carbon atoms C 64 and C 67, polarized towards the carbon atoms (77.9%/22.1%) is present (NBO 161 and 165) with an occupancy of 1.93. Between the backbone nitrogen atoms N65 and N65 a double bond (NBO 162 and 163) is observed, together with a single bond towards the respective connected carbon atom (N66 – C67, NBO 164 and N65 – C64, NBO 160). On both sides of the molecule a double bond is present between the carbene carbon atoms C34 and C69 and the core carbon atoms C64 and C67 (NBO's 126 and 127; NBO's 166 and 167) with the π bond being polarized towards the core (62.3%/37.7%).

Second order perturbation theory analysis shows donor acceptor interaction (DAI) of the vinyl π bonds (C34 – C69; C64 – C67) into the empty p orbital on the germanium atom of 13.3 kcal mol^{-1} and 13.6 kcal mol^{-1} (NBO 127 → NBO 242; NBO 167 → NBO 242). Furthermore donation of the vinyl π bonds into the antibonding π* bond N65 – N66 is present with 29.2 kcal mol^{-1} each (NBO 127 → NBO 322; NBO 167 → NBO 322). In reverse, donation into the C-C π* orbitals (C34 – C69; C64 – C67) of 11.87 and 11.69 kcal mol^{-1} from the N65 – N66 π bond is observed (NBO 163 → NBO 286; NBO 163 → NBO 326).

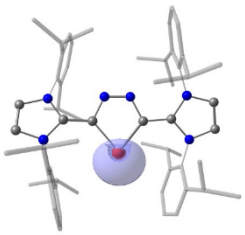

NBO 81
LP (Ge^{68}), occ. 1.97
82.7% s

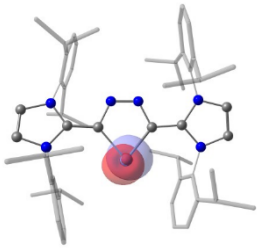

NBO 242
LV (Ge^{68}), occ. 0.48
99.7% p

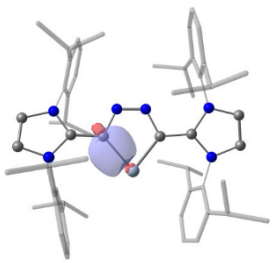

NBO 161
σ(C^{64}-Ge^{68}), occ 1.94
77.9% C^{64} ($sp^{1.65}$),
22.1% Ge^{68} (90.5% p)

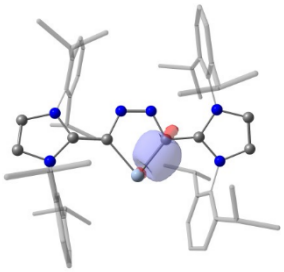

NBO 165
σ(C^{67}-Ge^{68}), occ 1.94
77.9% C^{67} ($sp^{1.67}$)
22.1% Ge^{68} (90.4% p)

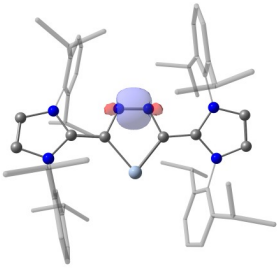

NBO 162
σ(N^{65}-N^{66}), occ 1.99
$sp^{2.29}$

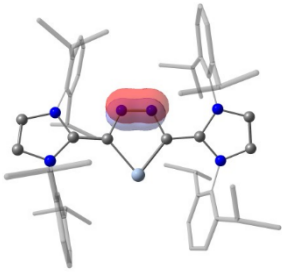

NBO 163
π(N^{65}-N^{66}), occ 1.91
99.8% p

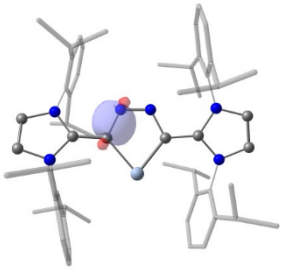

NBO 160
σ(C^{64}-N^{65}), occ 1.98
41.0% C^{64} ($sp^{2.50}$),
59.0% N^{65} ($sp^{1.92}$)

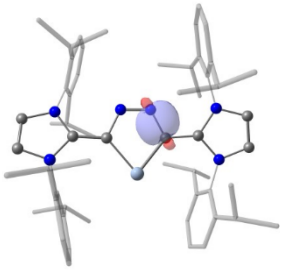

NBO 164
σ(C^{67}-N^{66}), occ 1.98
41.0% C^{67} ($sp^{2.52}$)
59.1% N^{66} ($sp^{1.90}$)

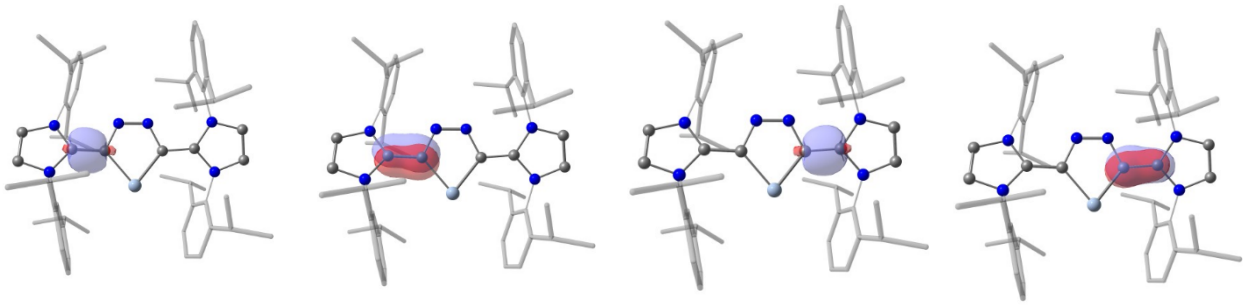

NBO 126	NBO 127	NBO 166	NBO 167
σ(C^{34}-C^{64}), occ 1.97	π(C^{34}-C^{64}), occ 1.65	σ(C^{67}-C^{69}), occ 1.97	σ(C^{67}-C^{69}), occ 1.98
53.4% C^{34} ($sp^{1.31}$)	38.2% C^{34} (99.9% p)	53.0% C^{69}($sp^{1.31}$),	37.7% C^{69} (99.9% p)
46.6% C^{64} ($sp^{1.96}$)	61.8% C^{64} (99.9% p)	47.0% C^{67}($sp^{1.94}$)	62.3% C^{67}(99.9% p)

Figure S43: Selected NBO's of compound **3**.

TD-DFT Calculations

TD-DFT calculations show that **1** is expected to have only one very low intensity transition in the visible region at 410 nm corresponding to the HOMO-LUMO transition. Similarly, **2** is also expected to have only one very low intensity transition in the visible region, at 411 nm, corresponding to the HOMO-LUMO transition.

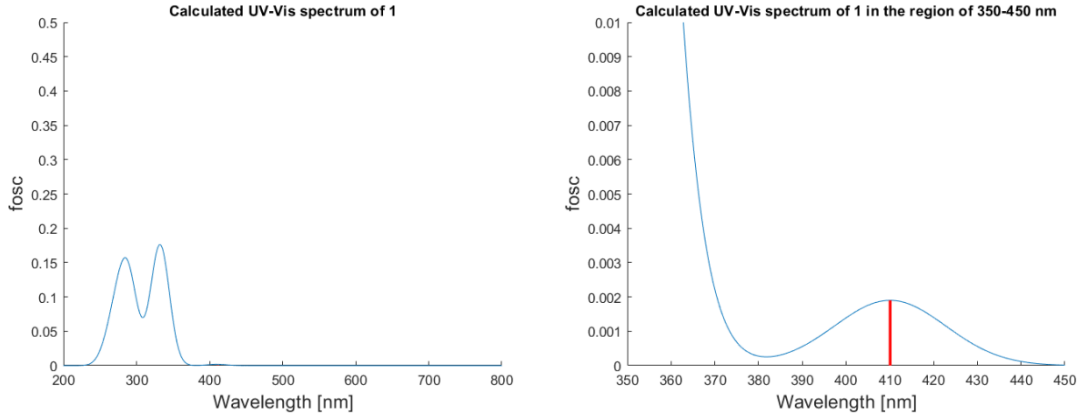

Figure S44: Simulated UV-Vis spectra of **1** at the regions of 200-800 nm (left) and 350-450 nm (right), based on TD-DFT calculations of the first 10 singlet excitations. The transition at 410 nm is shown as a vertical red line

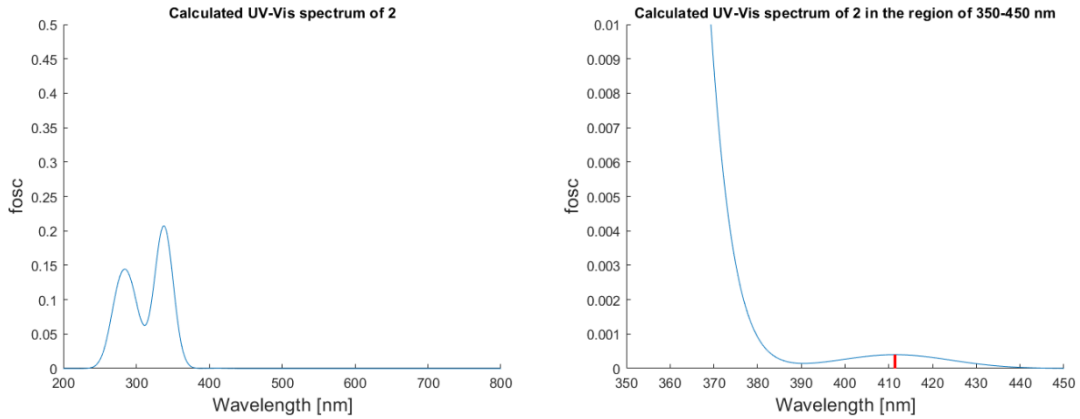

Figure S45: Simulated UV-Vis spectra of **2** at the regions of 200-800 nm (left) and 350-450 nm (right), based on TD-DFT calculations of the first 10 singlet excitations. The transition at 411 nm is shown as a vertical red line.

The orange/ beige colour of **1** and **2** could additionally originate from the hard-to-separate impurities found in the reaction mixture, such as **1'** and **2'**. While the $GeCl_3^-$ and $SnCl_3^-$ are not expected to have transitions in the visible region, the cation does have a transition at around 400 nm, which is also expected to be of higher intensity than that of **1** and **2**.

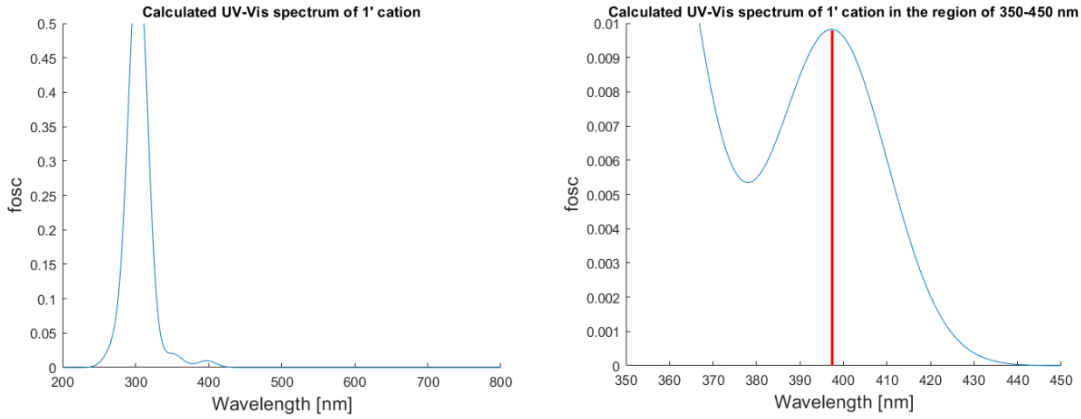

Figure S46: Simulated UV-Vis spectra of cation **1'** (or **2**') at the regions of 200-800 nm (left) and 350-450 nm (right), based on TD-DFT calculations of the first 10 singlet excitations. The transition at 397 nm is shown as a vertical red line.

TD-TDF calculation of **3** were also carried out. **3** exhibits three transitions on the visible region - at 436 and 406 nm with relatively high oscillator strengths, and at 409 nm with relatively low oscillator strength, corresponding to HOMO→LUMO, HOMO→LUMO+1 and HOMO-1→LUMO transitions respectively.

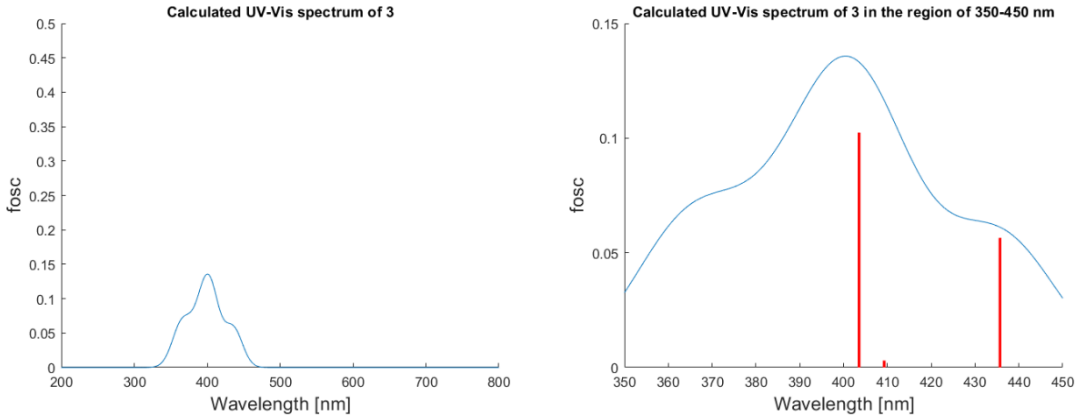

Figure S47: Simulated UV-Vis spectra of **3** at the regions of 200-800 nm (left) and 350-450 nm (right), based on TD-DFT calculations of the first 10 singlet excitations. The transition at 436, 409 and 406 nm are shown as a vertical red lines.

4. References

1 a) K. Powers, C. Hering-Junghans, R. McDonald, M. J. Ferguson and E. Rivard, *Polyhedron*, 2016, **108**, 8–14; b) R. K. Akhani, M. I. Moore, J. G. Pribyl and S. L. Wiskur, *J. Org. Chem.*, 2014, **79**, 2384–2396;

2 C. Kayser, R. Fischer, J. Baumgartner and C. Marschner, *Organometallics*, 2002, **21**, 1023–1030.

3 M. Muhr, P. Heiß, M. Schütz, R. Bühler, C. Gemel, M. H. Linden, H. B. Linden and R. A. Fischer, *Dalton Trans.*, 2021, **50**, 9031–9036.
4 P. Varava, Z. Dong, R. Scopelliti, F. Fadaei-Tirani and K. Severin, *Nat. Chem.*, 2021, **13**, 1055–1060.
5 APEX suite of crystallographic software, APEX 3 version 2015.5-2; Bruker AXS Inc.: Madison, Wisconsin, USA, 2015.
6 SAINT, Version 7.56a and SADABS Version 2008/1; Bruker AXS Inc.: Madison, Wisconsin, USA, 2008.
7 G. M. Sheldrick, *Acta Crystallogr. Sec. C.*, 2015, **71**, 3-8.
8 C. B. Hübschle, G. M. Sheldrick, B. J. Dittrich, *Appl. Cryst.,* 2011, **44**, 1281-1284.
9 G. M. Sheldrick, *SHELXL-97 – Program for crystal structure refinement*, University of Göttingen, Göttingen, 1998.
10 A. J. C. *Wilson, International Tables for Crystallography,* vol. C, Kluwer Academic Publishers: Dordrecht, The Netherlands, 1992, Tables 6.1.1.4 (pp. 500-502), 4.2.6.8. (pp. 219-222), and 4.2.4.2 (pp. 193-199).
11 C. F. Macrae, I. J. Bruno, J.A. Chisholm, P. R. Edgington, P. McCabe, E. Pidcock, L. RodriguezMonge, R. Taylor, J. van de Streek, P. A. J. Wood, *Appl. Cryst.,* 2008, **41**, 466-470.
12 O.V. Dolomanov, L. J. Bourhis, R. J. Gildea, J. A. K. Howard, H. Puschmann, *J. Appl. Cryst.,* **42**, 339 -341.
13 Gaussian 16, Revision C.01, M. J. Frisch, G. W. Trucks, H. B. Schlegel, G. E. Scuseria, M. A. Robb, J. R. Cheeseman, G. Scalmani, V. Barone, G. A. Petersson, H. Nakatsuji, X. Li, M. Caricato, A. V. Marenich, J. Bloino, B. G. Janesko, R. Gomperts, B. Mennucci, H. P. Hratchian, J. V. Ortiz, A. F. Izmaylov, J. L. Sonnenberg, D. Williams-Young, F. Ding, F. Lipparini, F. Egidi, J. Goings, B. Peng, A. Petrone, T. Henderson, D. Ranasinghe, V. G. Zakrzewski, J. Gao, N. Rega, G. Zheng, W. Liang, M. Hada, M. Ehara, K. Toyota, R. Fukuda, J. Hasegawa, M. Ishida, T. Nakajima, Y. Honda, O. Kitao, H. Nakai, T. Vreven, K. Throssell, J. A. Montgomery, Jr., J. E. Peralta, F. Ogliaro, M. J. Bearpark, J. J. Heyd, E. N. Brothers, K. N. Kudin, V. N. Staroverov, T. A. Keith, R. Kobayashi, J. Normand, K. Raghavachari, A. P. Rendell, J. C. Burant, S. S. Iyengar, J. Tomasi, M. Cossi, J. M. Millam, M. Klene, C. Adamo, R. Cammi, J. W. Ochterski, R. L. Martin, K. Morokuma, O. Farkas, J. B. Foresman, and D. J. Fox, Gaussian, Inc., Wallingford CT, 2016.
14 (a) A. D. Becke, *J. Chem. Phys.* 1993, **98**, 5648–5652.; (b) Lee; Yang; Parr, *Phys. Rev. B,* 1988, **37**, 785–789; (c) S. H. Vosko, L. Wilk, M. Nusair, *Can. J. Phys.*, 1980, **58**, 1200– 1211.
15 (a) R. Ditchfield, W. J. Hehre, and J. A. Pople, *J. Chem. Phys.*, 1971, **54**, 724; (b) W. J. Hehre, R. Ditchfield, and J. A. Pople, *J. Chem. Phys*., 1972, **56**, 2257; (c) P. C. Hariharan and J. A. Pople, *Theor. Chem. Acc*., 1973, **28,** 213-22; (d) P. C. Hariharan and J. A. Pople, *Mol. Phys.*, 1974, **27**, 209-
14; (e) M. M. Francl, W. J. Pietro, W. J. Hehre, J. S. Binkley, D. J. DeFrees, J. A. Pople, and M. S. Gordon, *J. Chem. Phys.*, 1982, **77**, 3654-65; (f) J.-P. Blaudeau, M. P. McGrath, L. A. Curtiss, and L. Radom, *J. Chem. Phys.*, 1997, **107**, 5016-21; (g) A. J. H. Wachters, *J. Chem. Phys.*, 1970, **52**, 1033; (h) L. A. Curtiss, M. P. McGrath, J.-P. Blaudeau, N. E. Davis, R. C. Binning Jr., and L. Radom, J. *Chem. Phys.*, 1995, **103**, 6104-6113; (i) M. Swart, M. Güell, J. M. Luis, and M. Solà, *J. Phys. Chem. A*, 2010, **114**, 7191 - 7197.
16 (a) R. Baierl, A. Kostenko, F. Hanusch and S. Inoue, *Dalton Trans.*, 2021, **50**, 14842–14848.
(b) S. Huzinaga, J. Andzelm, M. Klobukowski, E. RadzioAndzelm, Y. Sakai and H. Tatewaki. Gaussian Basis Sets for Molecular Calcuations, Elsevier: Amsterdam, 1984.
17 (a) E. D. Glendening, J, K. Badenhoop, A. E. Reed, J. E. Tischler J. A. Bohmann, C. M. Moral, P. Karafiloglou C. R. Landis and F. Weinhold, Theoretisches Chemieinstitut, University of Wisconsin, Madison (2018).
(b) E. D. Glendening, C. R. Landis and F. Weinhold, *J. Comput. Chem.,* 2019, **40**, 2234-2241.
18 Chemcraft - graphical software for visualization of quantum chemistry computations. Version 1.8, build 654. https://www.chemcraftprog.com